RECLAMATION

Managing Water in the West

Evaluation of Solar-Powered Systems for Desalination of Brackish Groundwater

Research and Development Office
Science and Technology Program

Final Report ST-2015-1340-1

U.S. Department of the Interior
Bureau of Reclamation
Research and Development Office

September 2015

Mission Statements

The U.S. Department of the Interior protects America's natural resources and heritage, honors our cultures and tribal communities, and supplies the energy to power our future.

The mission of the Bureau of Reclamation is to manage, develop, and protect water and related resources in an environmentally and economically sound manner in the interest of the American public.

Final Report ST-2015-1340-1

Evaluation of Solar-Powered Systems for Desalination of Brackish Groundwater

Research and Development Office
Advanced Water Treatment

by

Katie Guerra

and

Julie Korak

U.S. Department of the Interior
Bureau of Reclamation
Technical Service Center
Denver, Colorado

September 2015

REPORT DOCUMENTATION PAGE		*Form Approved* *OMB No. 0704-0188*
T1. REPORT DATE October 2015	**T2. REPORT TYPE** Research	**T3. DATES COVERED** October 2013 to September 2015
T4. TITLE AND SUBTITLE Evaluation of Solar-Powered Systems for Desalination of Brackish Groundwater		**5a. CONTRACT NUMBERS** 14XR0680A1-RY1541AW201421340 15XR0680A1-RY1541AW201521340
		5b. GRANT NUMBER
		5c. PROGRAM ELEMENT NUMBER 1340 (S&T)
6. AUTHOR(S) Katie Guerra Julie Korak		**5d. PROJECT NUMBER** 1340
		5e. TASK NUMBER
		5f. WORK UNIT NUMBER 86-68190
7. PERFORMING ORGANIZATION NAME(S) AND ADDRESS(ES) Katie Guerra, Bureau of Reclamation Julie Korak, Bureau of Reclamation		**8. PERFORMING ORGANIZATION REPORT NUMBER**
9. SPONSORING / MONITORING AGENCY NAME(S) AND ADDRESS(ES) Research and Development Office U.S. Department of the Interior, Bureau of Reclamation, PO Box 25007, Denver CO 80225-0007		**10. SPONSOR/MONITOR'S ACRONYM(S)** R&D: Research and Development Office BOR/USBR: Bureau of Reclamation DOI: Department of the Interior
		11. SPONSOR/MONITOR'S REPORT NUMBER(S) 2015-01-1340

12. DISTRIBUTION / AVAILABILITY STATEMENT
Final report can be downloaded from Reclamation's website: https://www.usbr.gov/research/

13. SUPPLEMENTARY NOTES

14. ABSTRACT *(Maximum 200 words)*

This Science and Technology Program research project focused on evaluating photo-voltaic powered reverse osmosis. Through the project, a basic version of photovoltaic reverse osmosis was constructed using a commercially available reverse osmosis unit and photovoltaic panels from a local hardware store.

The system was tested under controlled operating conditions with respect to water quality and recovery at two different locations: the Brackish Groundwater National Desalination Research Facility (BGNDRF) in Alamogordo, New Mexico (NM), and the Denver Federal Center in Denver, Colorado (CO). Measurements were taken throughout the testing period recording permeate flow, water quality (i.e., conductivity, pH, and temperature) and global horizontal irradiance (GHI) using a pyranometer. The system was also tested with different panel bearings and inclination angles, geographic location to show methods for analyzing data that accounts for these differences in solar conditions.

15. SUBJECT TERMS
renewable energy, desalination, reverse osmosis, nanofiltration, water treatment, economics, design

16. SECURITY CLASSIFICATION OF:			**17. LIMITATION OF ABSTRACT**	**18. NUMBER OF PAGES**	**19a. NAME OF RESPONSIBLE PERSON**
			U		Katie Guerra
a. REPORT U	**b. ABSTRACT** U	**c. THIS PAGE** U		77	**19b. TELEPHONE NUMBER** 303-445-2013

Final Report 2015-01-1340

Evaluation of Solar-Powered Systems for Desalination of Brackish Groundwater

Peer Review Documentation

Project and Document Information

Project Name Evaluation of Solar-Powered Systems for Desalination of Brackish Groundwater

Document _____ WOID Z1430

Peer Reviewer Anthony Kennedy Document Date September 2015

Review Certification

Peer Reviewer: I have reviewed the assigned items/sections(s) noted for the above document and believe them to be in accordance with the project requirements, standards of the profession, and Reclamation policy.

Peer Reviewer Anthony Kennedy /s/ Date _____
(Signature)

Disclaimer

The views, analysis, recommendations, and conclusions in this report are those of the authors and do not represent official or unofficial policies or opinions of the United States Government and the United States takes no position with regard to any findings, conclusions, or recommendations made. As such, mention of trade names or commercial products does not constitute their endorsement by the United States Government.

Executive Summary

Solar-powered desalination technologies can be used to treat non-traditional water sources to increase water supplies in rural, arid areas, of the southwestern United States (U.S.). Abundant solar resources combined with large amounts of brackish groundwater can make the coupling of solar power and desalination an attractive alternative to water supplies in areas without access to grid electricity.

A range of solar driven desalination processes have been developed. Some processes convert solar energy into electrical energy; whereas, others utilize produce thermal energy. Optimization of membrane separation processes may utilize solar energy in multiple forms, such as generating electrical energy via photovoltaic (PV) panels combined with solar thermal preheating of feed water. There is currently no standardized method to objectively compare treated water output and solar energy input. The objective of this study is to evaluate different method of quantifying solar energy input and its effect on water treatment for a PV reverse osmosis (PVRO) system with the goal of developing a characteristic system operating curve.

A PVRO system was built using readily available commercial components. The system consisted of PV panels, a pump controller, pump, and two reverse osmosis membranes in series. This simple system was used to also provide a benchmark of PVRO technology that other improvements in system design and operational optimization can be compared on the basis of both performance and cost.

The system was tested under controlled operating conditions with respect to water quality and recovery at two different locations: the Brackish Groundwater National Desalination Research Facility (BGNDRF) in Alamogordo, New Mexico (NM), and the Denver Federal Center in Denver, Colorado (CO). Measurements were taken throughout the testing period recording permeate flow, water quality (i.e., conductivity, pH, and temperature) and global horizontal irradiance (GHI) using a pyranometer. GHI is the total irradiance (both direct and diffuse) incident on a horizontal surface. The system was also tested with different panel bearings and inclination angles.

Using the PV panel location and orientation, an isotropic solar model was applied to quantify the solar irradiance on the PV panel based on the position of the sun relative to the PV panel at the time of sampling. Terms were systematically added to the isotropic model to evaluate the importance of modeling direct, diffuse, and reflective radiation. An isotropic solar model, including both the direct and diffuse solar radiation components (neglecting reflectance), was necessary to normalize the water production for systems with different panel orientations. After estimating the direct and diffuse components relative to the panel, the global irradiance on a tilted surface (GTI) was calculated to estimate the solar energy input to the system.

A characteristic operating curve relating permeate production as a function of solar energy input to the tilted panels ([GTI] x panel area) is shown in figure E1. With the application of the isotropic solar model, permeate production can be modeled within 20 percent given a GHI pyranometer reading under constant operating conditions (recovery and water quality). These results demonstrate the need for estimating the solar irradiance on a tilted solar collector [GTI] (considering orientation to the sun) and not report only GHI, as is commonly done.

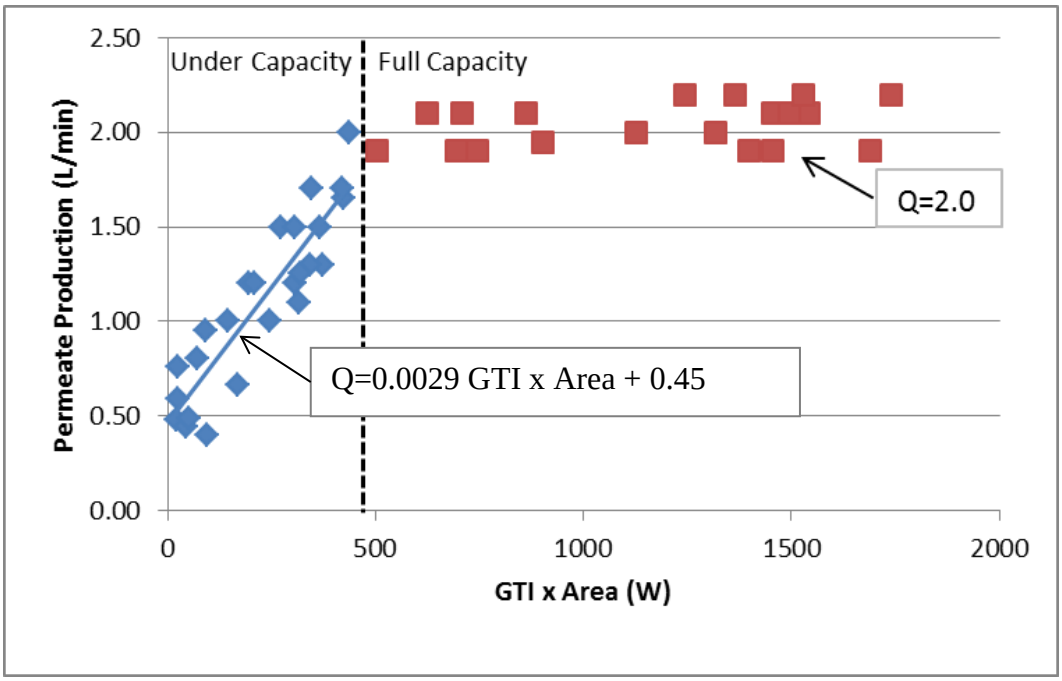

Figure E1.—Characteristic operating curve relating solar energy input (GTI x area) and permeate production.

Characterizing the performance of a solar-powered desalination process by relating solar energy input to water production has advantages over current methods. By quantifying the energy input to the inclined solar collector to determine the rate of energy input (watt (W) to panel rather than GHI alone) provides enough data for others to predict how a system would perform at a different geographical location or panel orientation. This method also quantifies performance by quantifying the solar energy input rather than intermediate parameters, such as electrical power generation. This basis allows systems that utilized different forms of solar energy to be compared directly.

The case studies performed in this project present one method of relating solar energy input to water production. While the need for adequately quantifying solar energy input is established in this study, additional work is needed to adapt the

method to other technologies. Relating the rate of energy input (W) to the rate of water production (L/min) was effective for the PVRO system due to a fast process response time. Alternative approaches need to be determined for processes that store thermal energy and have lag times between changing light conditions and permeate production. In any case, a standardized approach is needed that better relates water production to actual solar input rather than the practice of reporting pyranometer GHI readings.

Contents

Figures

Tables

Acronyms and Abbreviations

AC	alternating current
BGNDRF	Brackish Groundwater National Desalination Research Facility, Alamogordo, NM
BDL	Below detection limit
CO	Colorado
DC	direct current
DHI	diffuse horizontal irradiance
DNI	direct normal irradiance
DTI	diffuse irradiance on tilted surface
DWPR	Desalination and Water Purification Program
ED	electrodialysis
EDR	electrodialysis reversal
El	elevation
EPA	Environmental Protection Agency
Eqn	equation
ft	foot/feet
GFD	gallons per square foot per day
GHI	global hemispherical irradiance on horizontal surface
gpm	gallons per minute
GTI	global irradiance on tilted surface
HOMER	Hybrid Optimization Model for Multiple Energy Resources
Hp	horse power
hPa	hectopascals
hrs/d	hours per day
I_t	direct irradiance on a tilted surface
Kt	Total Clearness Index
L/d	liters per day

L/min	liters per minute
m	(air) mass
NM	New Mexico
NREL	National Renewable Energy Laboratory
Octa	measure of cloud cover at a given location
p	pressure
PV	photovoltaic
PVRO	photovoltaic reverse osmosis
ρ	surface albedo
R	reflective irradiance
Reclamation	Bureau of Reclamation
Rec	recovery
RO	reverse osmosis
ROSA	Reverse Osmosis System Analysis (software)
S&T	Science and Technology
SEC	specific energy consumption
SOLPOS	Solar Position and Intensity calculator
TDH	Total dynamic head
TDS	total dissolved solids
TSC	Technical Service Center
U.S.	United States
USGS	United States Geological Survey
UV	ultraviolet
W	watt
Z	solar zenith

1. Introduction

In rural areas of the western United States (U.S.), there is a need to develop robust, affordable desalination systems powered by renewable energy sources. Environmental conditions in many locations within the southwestern U.S. have abundant solar energy resources, making solar-powered desalination technologies an attractive solution for desalination in rural, off-grid areas.

Improving the efficiency of renewable energy-powered desalination systems is a focus area of Advanced Water Treatment within the Bureau of Reclamation (Reclamation). Reclamation has funded a number of solar-powered desalination studies. Research was conducted through the Desalination and Water Purification Program (DWPR), which funds externally conducted research and Reclamation's Science and Technology (S&T) Program. S&T funds Reclamation-employed research to conduct internal, applied research. Table 1 summarizes Reclamation-funded research in this area.

Table 1.—Summary of Reclamation-Funded Research in Solar-Powered Desalination

Type of System	Performing Entity	Years	Major Findings/Conclusions
PV-EDR	Reclamation	Mid-1990's	PV-powered EDR is a viable alternative for off-grid desalination. Project resulted in numerous conference proceedings and the filing of a patent (Lichtwardt and Williams, 2000). The patent has since expired due to failure to pay maintenance fees.
PVRO	ITN Energy Systems, Inc. (funded by DWPR)	2002-2003	Developed PVRO unit to produce water at 1.38 $kWhr/m^3$. The unit operated for 3 months on a water heavily dominant in calcium sulfate. Due to operation at an unrealistic recovery rate, the system was irreversibly fouled with calcium sulfate precipitation. The report concluded that careful control of recovery is critical to long term operation of a PVRO unit (Cheah, 2004).
Solar-Membrane Distillation	Reclamation/ University of Arizona	2011-2015 (on-going)	This project developed a solar-powered membrane distillation unit to provide livestock with water in the Navajo Nation. Membrane distillation was found to be easy to integrate with a hybrid solar-thermal-PV power generation system to produce water efficiently. This project is on-going at the time of publication of this report, so no final conclusions are available.
Solar Distillation	KII Inc. (funded by DWPR)	2010-2013	A new, efficient design was developed to improve upon the concept of classic solar distillation.
PV-EDR	Cal Poly Pomona (funded by DWPR)	2014-2015 (on-going)	A new control system and configuration for PV-powered electrodialysis is being developed. This project was on-going at the time this report was published, so no final conclusions are available.

PV-EDR = photovoltaic electrodialysis reversal
PVRO = photovoltaic reverse osmosis

Each of these research projects was successful in gathering data to show the performance of the renewable-energy powered desalination system. Because these systems are inherently different in their desalination mechanism, physical operation, driving force for separation, and require thermal or electrical energy, comparison of different technologies was difficult. Furthermore, the inherently unpredictable supply of solar energy that is dependent on geographic location, season, and weather events, adds to the complexity of comparing different systems tested in different locations at different times of the year.

The intent of this project was to provide a basis or methodology that can be used to facilitate the collection of a robust data set for solar-powered desalination technologies such that those data can be used to compare different types of systems and to predict the performance of one system under different conditions. The ability to predict the performance of a solar powered desalination technology under different solar conditions is critical for designing a water treatment system that is capable of supplying water reliability for a remote area.

2. Background

Desalination technologies are a key component to supply fresh water. The use of desalination is increasing as traditional water supplies become fully allocated due to the increasing demand for fresh water; the supply of fresh water resources is less predictable due to climate change and drought. Figure 1 shows that the majority of the water-stressed watersheds are in the western United States [Averyt et al., 2013].

Even in areas with a limited supply of fresh surface water there is often abundant groundwater and brackish (saline) groundwater. Desalination of brackish water offers some clear advantages over traditional water supply alternatives in rural, arid areas. Building reservoirs and pipelines is costly and carries significantly environmental impacts. Whereas, desalination of a locally available brackish groundwater increases the local control over the water supply and decreases the need for expensive infrastructure and high energy costs of conveying water over long distances. Desalination, however, does present some challenges, namely the high energy requirement for separating ions from water and the high cost, environmental impacts, and regulatory challenges of disposing of the concentrated brine.

The salinity of brackish groundwater is typically much lower than that of seawater and is present at relatively shallow depths, making pumping and desalinating groundwater a practical approach to augmenting fresh water resources. Figure 2 shows the location and depth of brackish water in the United States. From figure 2 it can be seen that there is some overlap between the areas with water stress (from figure 1) and areas with relatively shallow brackish groundwater.

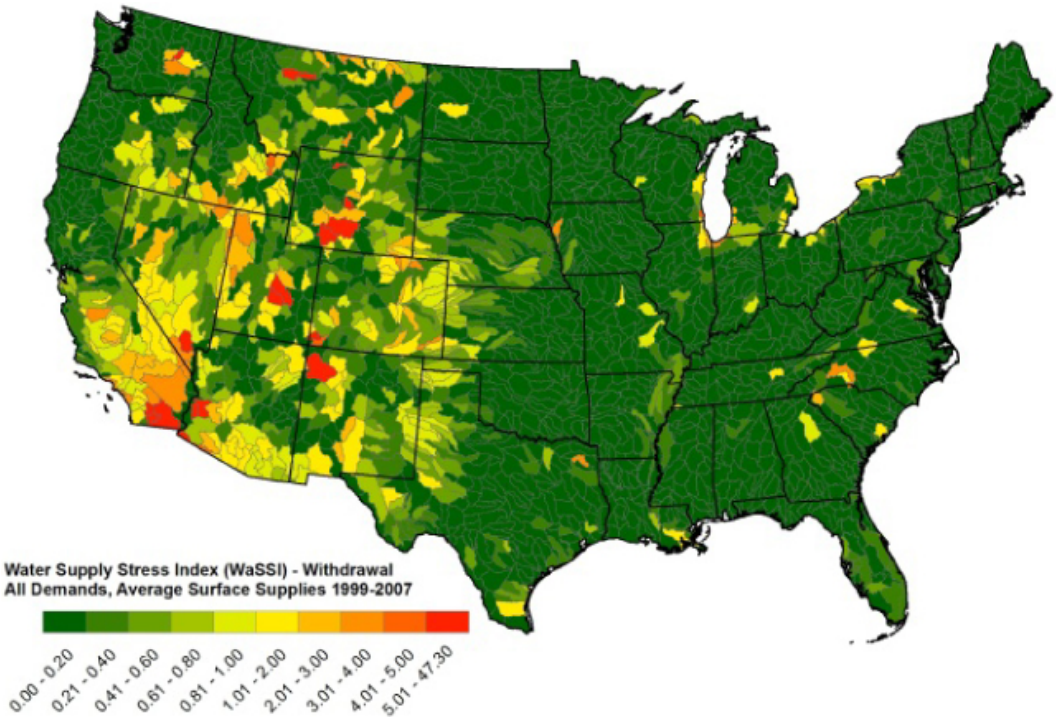

Figure 1.—Areas of water stress in the U.S. [Averyt et al., 2013].

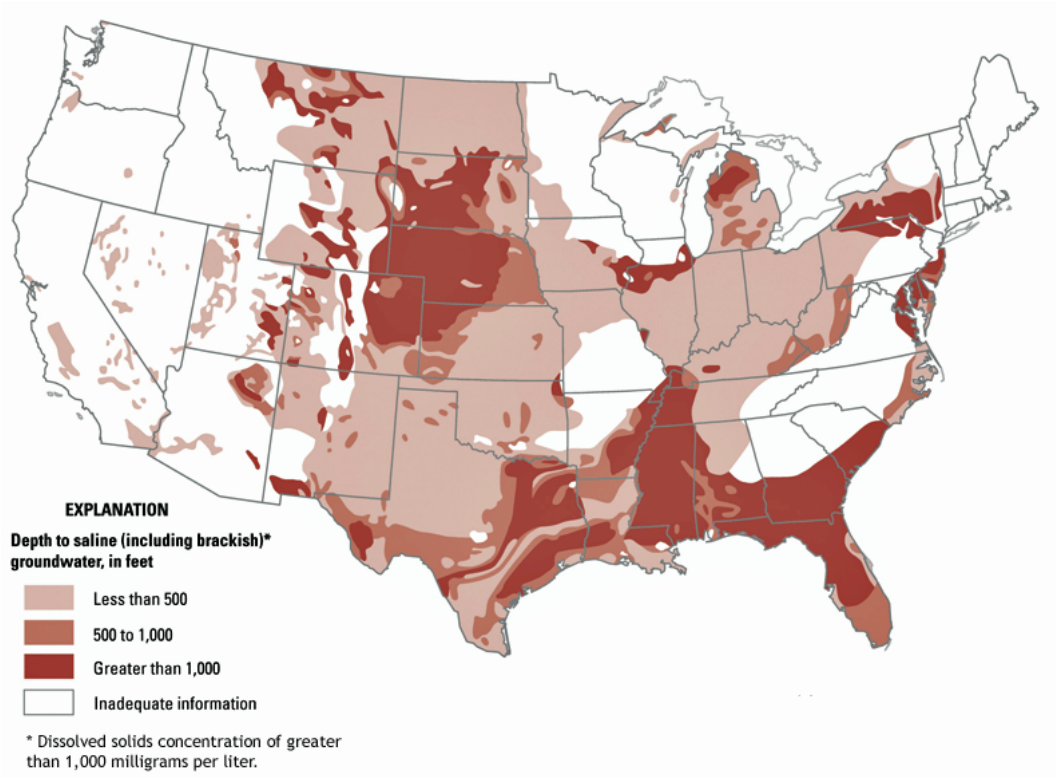

Figure 2.—U.S. brackish groundwater resources; depth to brackish groundwater. Image: U.S. Geological Survey (USGS) National Brackish Groundwater Assessment.

Because desalination processes are inherently energy intensive, there is interest in powering desalination using renewable energy resources. Most parts of the southwestern U.S. have abundant solar resources. The National Renewable Energy Laboratory (NREL) estimates the potential of renewable energy electricity generation; figure 3 and figure 4 show the availability of the PV power resource and the concentrating solar-power resource for the U.S., respectively. The southwestern states show the highest potential for generating electricity using photovoltaic (PV) and concentrating solar generating technologies (e.g., heliostats).

Considering the need for additional water supplies due to water stress, the availability of brackish groundwater, and the abundance of solar-power resources in the southwestern United States, there is a compelling case for the investigation of solar-powered desalination of brackish groundwater.

For desalination systems in areas with access to grid supplied electricity, the use of renewable energy can be used to offset power consumed by desalination. These systems utilize grid-tied renewable energy generation systems. The engineering and design of these systems is standard and does not depend on the use of the power, since it acts as another load on the grid. However, for small, remote communities where access to adequate, reliable, grid-supplied electricity is limited, there is a need to identify efficient ways of powering desalination technologies directly with renewable energy.

Because of the high cost of renewable energy generation and the large power requirement of desalination, there is an interest in identifying more efficient ways of coupling these technologies that can provide increased performance over simply connecting a PV power source to a desalination technology. This report provides an overview of solar-powered desalination technologies and identifies considerations for testing and data reporting for the evaluation of these technologies.

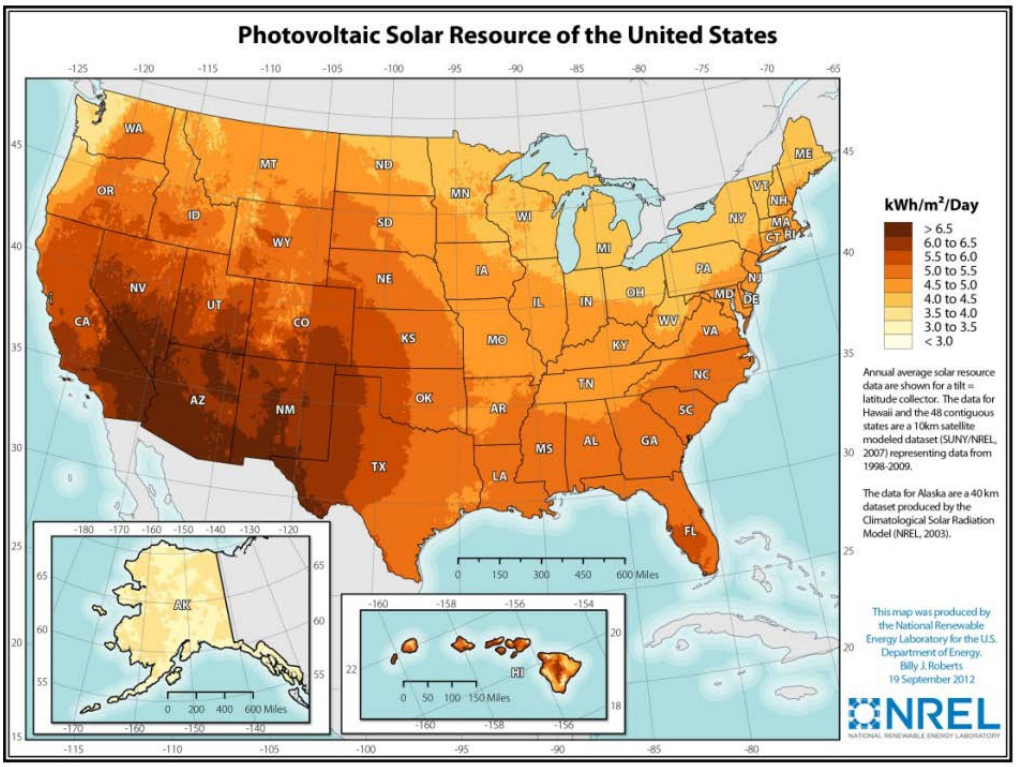

Figure 3.—Availability of solar-PV resources in the U.S.

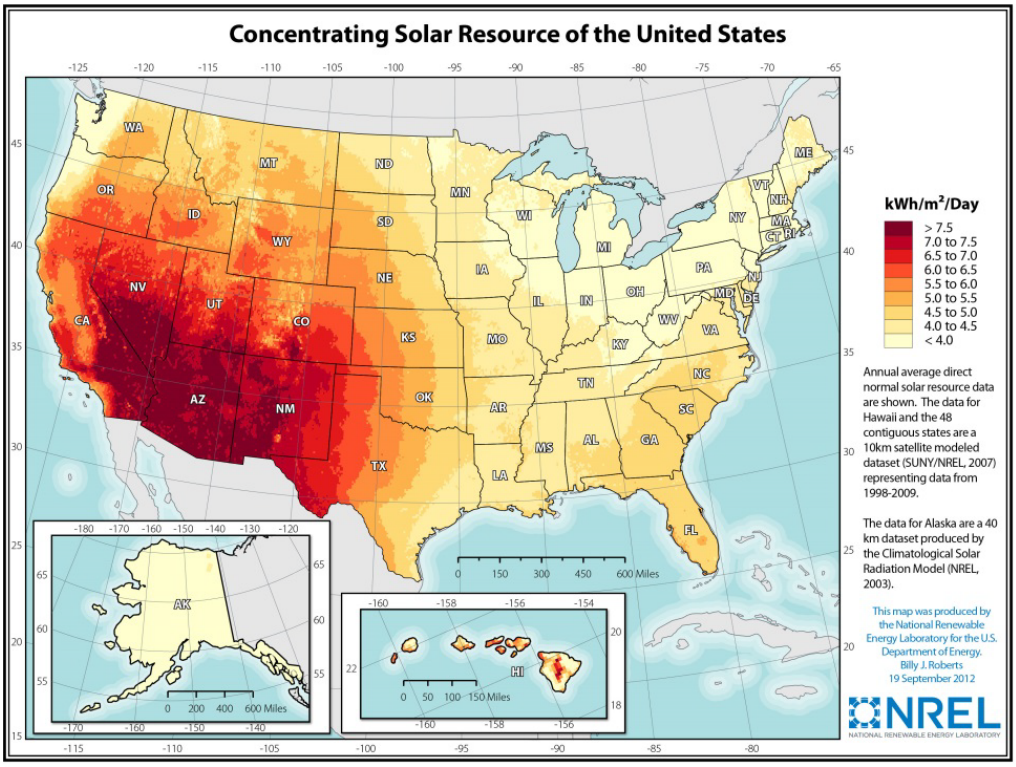

Figure 4.—Availability of concentrating solar resource in the U.S.

3. Review of Solar-Powered Desalination Technologies

Solar-powered desalination encompasses a broad range of technologies that use solar energy in some form to desalinate water (figure 5). Renewable energy can be harnessed in many ways to drive desalination processes. One straightforward approach is converting renewable energy to electricity using PV cells and using the electricity to power the desalination process. However, significant energy losses occur during the conversion of solar energy to electricity. Other methods of using solar energy for desalination include concentrating and non-concentrating solar thermal processes. In each case, collectors convert solar radiation to thermal energy that can subsequently be used to drive separation processes. To optimize the desalination processes, hybrid systems that use more than one renewable energy source have been proposed. Some hybrid systems couple PV electricity generation with other renewable sources of electricity (e.g., wind turbines) [Ghermandi and Messalem, 2009]. While some researchers have found hybrid renewable energy systems consisting of wind and solar power to be more cost effective [Bourouni, M'Barek, and Taee, 2011], combining two renewable energy systems increases the complexity of the electrical control equipment. Some hybrid systems may employ a different form of solar energy using both solar thermal and PV solar collectors [Kelley and Dubowsky, 2013]. In any solar-powered desalination system, solar irradiance on the solar collector is the driving force behind the process.

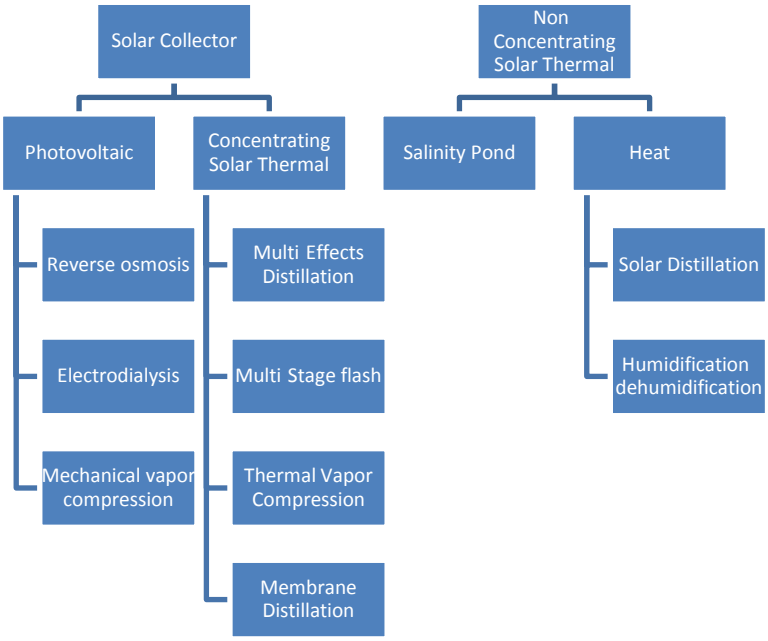

Figure 5.—Common pairings of solar energy and desalination.

While a range of renewable energy sources are of interest for developing sustainable desalination processes, this report focuses on the use of solar energy resources to provide electrical power to desalination technologies. Due to the potential for utilizing synergies between solar energy harvesting and desalination, solar-powered desalination has been an area of increasing research over the last 20 years (figure 6). Even though the capital costs associated with PV are considered to be relatively high, the long lifespan and low maintenance make PV a preferred renewable energy source for coupling with desalination technologies [Essam S. Mohamed and Papadakis, 2004]. PV can be used to power virtually any type of water treatment equipment. The most commonly reported PV-powered desalination technologies in the literature are reverse osmosis (RO) and electrodialysis (ED) (or electrodialysis reversal (EDR)).

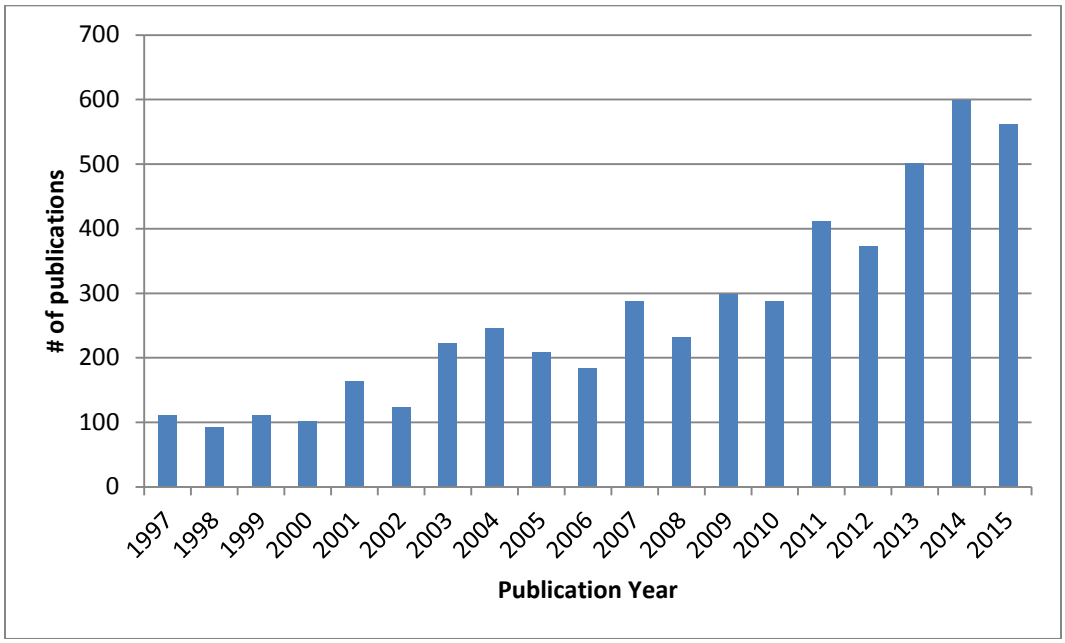

Figure 6.—Science Direct search results per year for “solar-powered desalination.”

Within the category of solar-powered desalination, this report focuses on PV coupled with reverse osmosis (PVRO), because it involves two readily available technologies. Off-the-shelf components are easily available online and at local hardware stores. Therefore, this technology was used as a benchmark for the performance and cost of renewable energy powered desalination, which can be used to compare future technological improvements and different types of solar-powered desalination technologies. In order to compare different types of solar-powered desalination processes, determining system performance (i.e., water production) relative to solar energy input is an important first step. This report also presents a methodology that can be used to collect data for comparing system performance relative to actual solar energy available to a solar collector and can be the basis for comparisons between different types of systems and different

testing locations. Therefore, the results of this report are applicable to a wide range of applications and technologies.

3.1 PVRO System Overview and Design

System design and operation of PVRO requires consideration for both the desalination and energy production requirements to meet the desalination goals (both water quantity and quality), see table 2. In its simplest form, PVRO consists of a membrane desalination unit, PV panels, and an electrical pump controller. The PV panels generate electricity. The pump controller moderates the power sent to the membrane desalination unit, which consists of a pump, membrane elements, and associated instrumentation. Additional components, such as batteries, chemical feed systems, and energy recovery systems, may also be included.

Equipment sizing of the membrane system and the PV system are critical for cost effective implementation of PVRO. For stand-alone systems powered entirely by solar energy, the power supply is intermittent as opposed to systems powered by grid electricity. Systems operating with a constant supply of relatively inexpensive grid electricity are typically sized to reduce the cost of the water treatment equipment and often times operate continuously 24-hours per day. However, due to the intermittent nature of solar energy, sizing of the water treatment system and the electricity generating and storage systems are more complex and must account for shorter operating times. The following sections provide some guidance on design and sizing of the individual components of the PVRO system.

Table 2.—PVRO System Components

Equipment	Purpose	Required or Optional
PV array	Converts sunlight to electricity	Required
Electrical system controller	Regulates energy produced by PV panels, allows for system shutoff during low power, and optimizes pump efficiency under low-light conditions	Required
Batteries	Provides energy storage which allows for longer sustained operation or for more consistent operation of PVRO	Optional
Charge controller	Maintains battery charge	Optional (required if using batteries)
DC-AC inverter	Converts DC power from PV to AC for use by system equipment (pumps, instrumentation, etc.)	Optional depending on type of pump and equipment used
Reverse osmosis unit	Water desalination production equipment: pumps, membranes, backpressure valve	Required

Equipment	Purpose	Required or Optional
RO system instrumentation	Manual or automated instrumentation for collecting data on system performance (flow rate, water conductivity, system pressure)	At a minimum, manual gauges and grab samples to ensure suitable product water quality are required. Other instrumentation is optional.
Chemical feed systems	Reduces the potential for precipitation of sparingly soluble salts in RO system; typically pH adjustment or antiscalant addition	Optional
Energy recovery device	Recovers mechanical energy from high pressure RO concentrate stream to assist with pressurization of feed	Optional
Concentrate management	System to handle highly saline concentrate water produced from PVRO	Optional

3.1.1 RO System Design

The standard method for designing an RO system is to use software packages provided by membrane manufacturers that model water recovery, salt rejection, and power requirements. A membrane system should be designed to operate within the manufacturer recommended ranges to minimize the rate of organic and inorganic fouling and to eliminate the potential for mechanical damage to the system. Membrane operating conditions are limited by the maximum membrane recovery, maximum operating pressure, maximum permeate flow, maximum feed water flow rate, and the minimum concentrate flow rate [Dow, 2008].

The design process starts by determining the volume of treated water required per day. Since the default of most software programs is to produce the desired product water over 24 hours, adjustments are required in modeling to account for the periodic operation of the system. The user should adjust the flow rate to match the number of hours of planned operation each day. For example, if 1,000 liters per day (L/d) of product water is required to be produced by a PVRO system and the system operates for only six (6) hours-per-day, the specified flow rate should be four (4) times higher than the flow rate based on 24 hours of operation (e.g., 4,336 liters per minute (L/min) rather than 1,084 L/min).

Specification of permeate flow rates along with feed water quality are software simulation inputs to determine appropriate membrane and pump selection. The user can select membrane materials and configurations while balancing desired product water quality and power requirements. The simulations also provide information regarding maximum operating conditions (e.g., recovery and pressure) to avoid scaling and membrane damage. By modeling the process water recovery, feed flow rate, and pressure, an appropriate pump and complimentary pump controller can be selected.

3.1.2 PV System Design

For systems operating remotely without access to grid electricity, all of the energy required to power the desalination system is produced by PV panels. Therefore, the PV system is designed and sized to supply 100 percent of the power demand from the RO system. The conversion efficiency, or the percentage of solar irradiance on a PV panel converted into electrical energy, is approximately 15 percent [Ghermandi and Messalem, 2009]. Determining the system capacity must take into account the available solar energy, the fraction of light incident on the panels and conversion efficiency to electricity.

The number of panels needed for a given desalination process depends primarily on the pumping requirements and estimated solar irradiance. The pumping power (kilowatt (kW) or kW/gal) is estimated by the membrane software simulation. It is important to further consider the effects of the pump controller on the PV panel outputs. This value can be used to determine the number of solar panels needed for the RO system operation. The controller will moderate the power sent to the pump. Oversizing the PV panels may produce more water during low-light conditions but may be wasted capacity during peak solar irradiance hours. The PV panel capacity should be confirmed after sizing the RO pump to ensure that the power estimate from the software simulation is consistent with the power required by the pump.

A key consideration with respect to the PV system is whether to send direct current (DC) or alternating current (AC) to the pump and other electrical components. PV panels generate DC current. If equipment requires AC, then an inverter is required at the expense of some energy loss. Approximately 5 to 15 percent of the power generated is lost in the conversion from DC to AC power. Therefore, there is a benefit to using DC pump motors for better utilization of the power generated. However, AC power is typically needed for instrumentation and control systems. To avoid the need for AC power, manual gauges can be used to monitor the system performance for water productivity and water quality.

Another consideration in the design of the PV system is whether or not to use batteries to increase water productivity. Batteries can be used for energy storage to extend the operational time of the RO system. Batteries may also help maintain constant operating conditions (i.e., pressure and flow) during fluctuating solar conditions (e.g., cloud events). Constant operating conditions are important for maintaining permeate water quality as some constituents (e.g., fluoride and nitrate) exhibit decreased rejection under low-flow conditions [Richards and Richards, 2011]. In addition to battery storage, advanced instrumentation and control systems used to control unit operation under variable solar conditions would represent another power demand from the system and benefit from constant power supply. However, it should be noted that added functionality also increases process complexity and cost.

Hybrid Optimization Model for Multiple Energy Resources (HOMER) can be used to optimize the sizing of PV and auxiliary equipment, such as batteries for a PVRO system. This allows the user to identify whether a hybrid system may offer a more cost effective PV design.

3.1.3 Optimized Design of PVRO

Some researchers have proposed more complex system design methodologies that incorporate optimization algorithms to optimize system design to minimize cost. These algorithms can take into account optimal sizing of the PV system relative to the RO system and water and power storage systems. Coupling the RO system optimization to the PV system optimization may provide a better solution than optimizing each system independently. At the time of this publication information was not available to compare the PVRO system design using a basic design approach, separate optimization of PV and RO, and a combined PVRO optimization algorithm.

3.2 Economic Evaluation of PVRO

PVRO has been shown to be an effective, affordable solution to water supply challenges for small-scale applications without access to grid electricity [Abdallah, Abu-Hilal, and Mohsen, 2005]. A wide range of costs for water production via PVRO have been reported: \$3.73/m^3 [Ahmad and Schmid, 2002], \$2.17/m^3 to \$2.43/m^3 [Bilton, Wiesman, Arif, Zubair, and Dubowsky, 2011], \$1.5 to \$6/m^3 [Garg and Joshi, 2014] and \$2.5/m^3 to \$40/m^3 [Ghermandi and Messalem, 2009]. The cost of PVRO varies greatly depending on the solar conditions and the water quality in the area the system will be installed. The cost of PVRO is very site specific, because the cost to implement this technology depends on the solar resources available and the type of feed water used for desalination.

In most PV power generation applications, battery storage represents a large capital cost and is often not used when another power source (e.g., gas generator) can accommodate power needs in the absence of solar energy. In the case of water treatment applications, the use of batteries warrants some consideration. Compared to the cost of the desalination system, battery cost may be less significant, but there is a trade-off between implementing batteries and sizing a larger system without batteries. Elasaad, et al., [2015] found that the PV/battery system accounted for 25 percent of the total capital cost of the system while the water treatment equipment (RO, cartridge filters, and ultraviolet (UV) disinfection) accounted for over 50 percent of the capital cost [Elasaad, Bilton, Kelley, Duayhe, and Dubowsky, 2015]. Several other studies have investigated the trade-off between cost and water production by incorporating batteries [Clarke, Al-Abdeli, and Kothapalli, 2013; Mohamed, Papadakis, Mathioulakis,

and Belessiotis, 2008]. Many studies have concluded that using batteries to store energy to extend operating time each day is less inefficient than producing more water during peak hours [Bilton, Kelley, and Dubowsky, 2011]. There may be additional operating conditions that justify some battery storage. Cloud events can cause rapid changes in power production that lead to a rapid change in pump output. These extreme fluctuations in flow and pressure can impact permeate water quality [Richards and Richards, 2011] and compromise membrane integrity. Some incorporation of battery storage to dampen these fluctuations warrants further investigation not solely from a cost perspective but from an operation stability perspective as well.

3.3 System Testing and Evaluation

Because PVRO productivity and cost is highly dependent on the conditions under which it is used and tested, comparing different systems tested or operated in different locations with different feed waters is difficult. The amount of water produced depends not only on the system components but also on how much solar irradiance strikes the panel (location and panel orientation), raw water quality and water recovery. While many of the references found in the literature describe how a system performs in a given location, very little information is available to assess how a given PVRO system will perform in a different location based on data collected in another location. This discrepancy makes inter-study comparisons difficult. Table 3 summarizes some of the PVRO literature.

To bypass the need to collect solar irradiance data, many PVRO studies evaluate performance by measuring electrical power generation and calculating the specific energy consumption (SEC) with units of kWh/m^3. This performance measure may be sufficient for PVRO studies, but technologies that use other forms of solar energy cannot be evaluated. For example, solar distillation cannot be evaluated as no electrical energy is generated. To optimize PVRO systems, hybrid systems have been developed that use solar thermal energy to preheat feed water [Kelley and Dubowsky, 2013; Khayet, Essalhi, Armenta-Déu, Cojocaru, and Hilal, 2010]. In these cases, the water production is a function of both the electricity generation by the PV panel, but also the effectiveness of the solar thermal system to preheat the feed solution. This is an example where quantifying the water production as a function of energy to the pump would not adequately characterize the efficiency of the system. Therefore, system efficiency should be evaluated by comparing the water produced to the incident solar energy on the various collectors.

Table 3.—Summary of PVRO Literature

Reference	Scope of Study	Test Info	Source Water	Water Production	Conclusion
Abdallah, et al, Desalination, 2005 [Abdallah et al., 2005]	PVRO testing and data collection, evaluated fixed versus east-west tracking	Jordan, April 5	Tap water, 400 mg/L TDS	0.18 L/min (tracking), 0.16 L/min fixed	12.5% increase in water production for tracking compared to fixed solar panels
Ahmad, Schmid, Energy Conversion and Management, 2002 [Ahmad & Schmid, 2002]	PVRO with battery, economic and physical model, power sizing and economic information	NA	NA	NA	PVRO cost of $3.73/$m^3$ (year 2000 cost basis).
Bilton et. al, Renewable Energy, 2011 [Bilton, Wiesman, et al., 2011]	PVRO, economic and physical model, Compared water produced using renewable energy and diesel	Many	Many	Many	PVRO more cost effective than diesel for all inland brackish desalination applications studied and a few seawater desalination applications (in areas with good solar resource availability)
Bourouni, et. al, Reneweble Energy 2011 [Bourouni et al., 2011]	PVRO with and w/o batteries, hybrid wind/PV RO, wind RO with batteries (simulation)	NA	NA	15 m^3/day	Presents sizing information and simulation results. Indicates preference for wind powered RO for application in Tunisia
El-Shaarawai, et al., Desalination, 2011 [El-Shaarawi, Al Awjan, Al Ramadhan, & Hussain, 2011]	Estimate system cost for PVRO (model)	NA	NA	NA	
Fiorenza, et al., Energy Conversion and Management, 2003 [Fiorenza, Sharma, & Braccio, 2003]	ST/MEE and PVRO	NA	NA	NA	5000 m3/d cost is approximately $2/$m^3$ and is ~2.5 times higher than conventional system, economy of scale realized from 1000 to 5000 m^3/d
Helal et al., Desalination 2008 [Helal, Al-Malek, & Al-Katheeri, 2008]	Evaluate 3 systems: diesel-powered RO, diesel/PV RO, and PVRO (model)	United Arab Emirates	Seawater	20 m^3/d	Optimal design depends on locational cost of energy, solar alternative become cost competitive at panel cost of $8/W
Herold, Neskakis, Desalination 2001 [Herold & Neskakis, 2001]	PVRO with batteries		Seawater	3 m^3/d, <500 mg/L	
Elasaad et al., Desalination, 2015 [Elasaad et al., 2015]	PVRO with batteries; testing and economic evaluation		Brackish water and rainwater	1 m^3/d, < 10 ppm TDS, 1000 L in 8 hr (well water), 6 hr (rain water)	Also had solar-powered UV, water cost = $9/$m^3$
[Garg & Joshi, 2014]	PV with RO, NF and RO/NF hybrid. Response surface modeling and economic analysis	N/A	Synthetic brackish water	Optimized recovery 12-18%. 0.8-3.7 m^3/d 41-322 mg/L TDS in permeate	9-19 kWh/m^3 specific energy capacity
[Clarke et al., 2013]	PVRO with and without battery	Australia	Synthetic 1-4% saline	10% recovery 0.1 m^3/d	11-14 kWh/m^3

Some studies have used pyranometers to measure solar irradiance in an effort to relate water production to available solar energy. There is no standardized method within the desalination field for reporting or using this data, which further complicates inter-study comparisons. Depending on how the meter is mounted affects the energy reading. When the meter is mounted at the same angle and orientation as a flat solar collector, the reading represents the global tilted irradiance (GTI) incident on the collector. When mounted horizontally, the reading represents the global hemispherical irradiance (GHI) and does not account for the position of the sun in the sky relative to the solar collector. Some studies mount the pyranometer at an incline [Nafey, Mohamad, El-Helaby, and Sharaf, 2007], others mount it horizontally [Khayet et al., 2010; Sathyamurthy, Kennady, Nagarajan, and Ahsan, 2014], and other studies do not specify the orientation [Sathyamurthy, El-Agouz, and Dharmaraj, 2015; Taghvaei et al., 2014]. If a pyranometer is mounted horizontally, the reading is not representative of the actual solar irradiance incident on the solar collector. This study investigates and proposes a standard method for relating water production to solar energy irradiance.

3.4 Inclined Plane Solar Collector Theory

Many solar-powered water treatment systems use inclined planes as solar collectors. Example systems include PV panels and solar distillation systems utilizing flat collectors [Kargar Sharif Abad, Ghiasi, Jahangiri Mamouri, and Shafii, 2013; Nafey et al., 2007]. To gauge the efficiency of a solar-powered water treatment system, it is necessary to quantify the energy input to the system. Solar energy input to any system depends on many environmental and system parameters. First, the available solar energy depends on how much energy reaches the Earth's surface at a given location, day, and time. Second, the orientation and geometry of the solar collector, with respect to the incoming solar radiation, dictates the fraction of solar radiation that is incident on the solar collector. This section presents the fundamental theory relating GHI pyranometer measurements to the actual energy available to an inclined solar collector.

The total irradiance that strikes a horizontal surface is termed the GHI and is the most common irradiance measurement documented. GHI can be measured directly using a pyranometer mounted on a horizontal surface or estimated using models. For example, the Bird Clear Sky Total Hemispherical Irradiance model estimates GHI based on geographical location, date, time and atmospheric conditions [Myers, 2013]. GHI represents the total intensity (direct and diffuse) on the horizontal surface [Kreider and Kreith, 1981]. Direct normal irradiance (DNI) is the solar radiation that arrives on a surface oriented normal to the solar beam. Radiation that has been scattered by the atmosphere before reaching a horizontal surface is termed diffuse horizontal irradiance (DHI). The relative contribution of the DNI and DHI components to a measured GHI depends on the

solar zenith (Z) according to equation (Eqn) 1. Z represents the angle of the sun relative to vertical (z-axis in figure 7). The Z angle can be calculated given the geographical location, date, and time [Kreider &and Kreith, 1981; Myers, 2013].

$$GHI = DNI\ cosZ + DHI \qquad \textbf{Eqn 1}$$

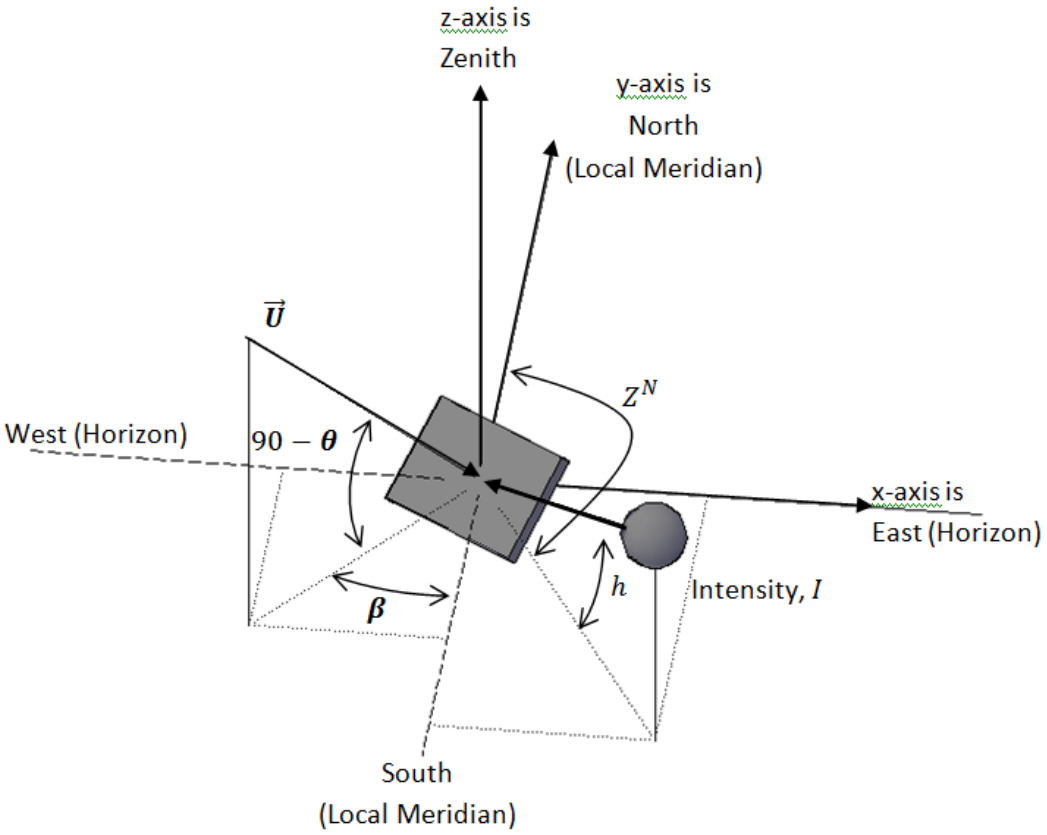

Figure 7.—Schematic for geometrical definitions for solar model.

The total solar energy that is available for the solar-powered water treatment system depends on the type and orientation of the solar collector. For example, a PV panel array can be represented as a tilted plane, and the solar radiation incident on the plane will depend on panel orientation relative to the sun. To illustrate with an exaggerated example, for the same GHI reading, the solar input to a PV panel array will be different if the direct component strikes the front or rear of the panel.

To determine the total solar input as GTI, the energy input depends on the direct irradiance on tilted surface (I_t), diffuse irradiance on tilted surface (DTI), and reflective irradiance (R) components that strike the inclined plane, according to Eqn 2. In addition to direct and diffuse components, a tilted plane will also receive reflected radiation from the surrounding surfaces. Since an array panel is tilted, the radiation incident on a panel arrays depends on two (2) important

geometrical parameters: the panel incline (β) and solar incidence angle (θ_i). The solar incidence angle is defined as the angle between the direct normal beam and a vector normal to the panel [Myers, 2013]. The incidence angle dictates what portion of the direct normal irradiance (DNI) strikes the array in the calculation of I_t. The panel incline dictates the DTI and R contributions. These fundamental equations demonstrate that the solar insolation on a flat solar collector depends on uncontrollable factors (e.g., GHI), as well as system specifications (e.g., panel orientation), and accounting for both is important to evaluate the efficiency of solar-powered water treatment systems.

$$GTI = I_t + DTI + R \qquad \text{Eqn 2}$$

4. Methods and Materials

4.1 PVRO Test System

The PVRO system used in this study was constructed using off-the-shelf components. The RO system was purchased from wateranywhere.com. The unit is a wall-mount system that was mounted inside of a box made of marine plywood. A wall-mounted system was used, because it is less expensive than a frame mounted system. The box was fabricated in the Technical Service Center (TSC) laboratory and was used to protect the system from environmental conditions in the field during operation. The system has a maximum production capacity of 1,200 gallons per day. Table 4 provides specifications for the RO system.

Table 4.—RO System Specifications

Parameter	Value
System model #	WM-225A
Maximum water production	1,200 gallons per day (based on 24 hrs/d)
# of membrane elements	2 (in series)
Membrane size	2.5” x 40” spiral wound
Membrane type	Thin film composite
Cartridge filter	5 to 30 um
Operating pressure range	40 to 175 psi

The RO unit came with a ½ horse power (hp) pump with an AC motor. Because of the increased efficiency of using the DC supplied by the PV array, a new pump with a DC motor was installed to replace the original pump supplied with the unit. The solar panels were connected to the pump using a pump controller that moderated the voltage and current sent to the pump. A complementary pump controller helps the pump operate in low-light conditions and prevent over-speed.

Between the three (3) case studies, two (2) different DC pumps and pump controllers were used. Specifications for each pump and pump controller are provided in each case study.

A small PV array was used to power the RO system (Grape Solar GS-S-100-TS). Each panel has a cell area of 0.5 m^2 with a peak power output of 100 watt (W). The PV panels were connected to the pump controller.

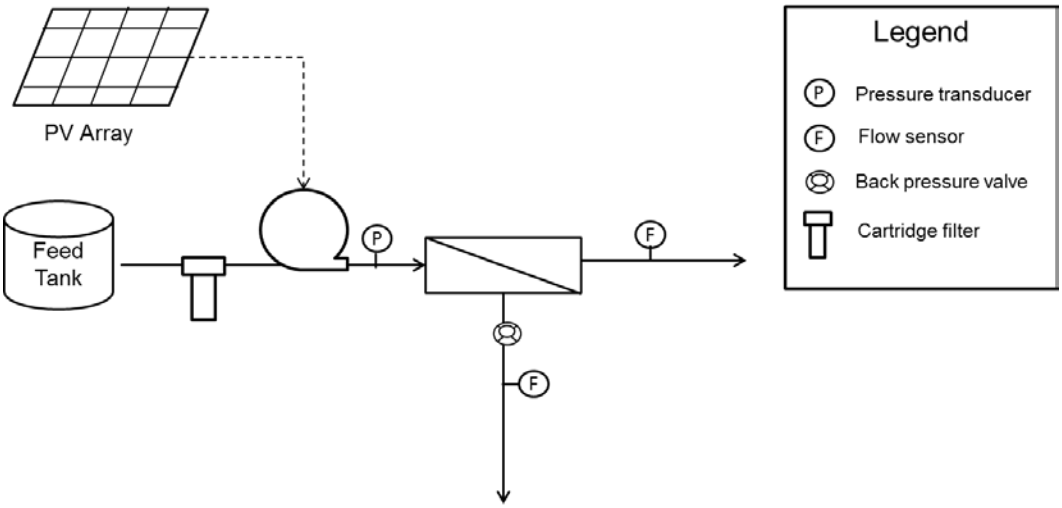

Figure 8.—Schematic diagram of PVRO system.

4.2 System Cost

The PVRO system costs were tabulated. Because the RO system was purchased as a package unit, the cost for all valves and plumbing are included in the cost of the RO system. PV panels were purchased from the local hardware store. The pump that came with the RO unit was replaced with a pump with a DC motor. The cost for labor to replace the pump, build a rack for the PV, and wire the PV to the motor is included. The tabulated costs in table 5 represent the installed cost for the PVRO system.

Table 5.—PVRO System Costs

System Component	Specification	Cost
RO system (wateranywhere.com)	(2) 2.5” x 40” spiral wound membranes	$2,400
PV (local hardware store)	Total power supply = 400 W	$1,800
Pump	1/5 hp, DC motor	$1,100
Labor	40 hrs @ $50/hr	$2,000
Total		$7,300

4.3 Membrane Selection

The software program Reverse Osmosis System Analysis (ROSA) software was used to identify membranes to be used in the PVRO unit. The ideal membrane requires a low operating pressure while meeting the target product water salinity requirements of 500 mg/L total dissolved solids (TDS). A range of membranes spanning the RO and NF range were investigated. The Brackish Groundwater National Desalination Research Facility (BGNDRF) in Alamogordo, New Mexico (NM) Well 3 water quality analysis, shown in table 11, was used as an input. Table 6 lists the values of the other parameters used to conduct the ROSA simulation.

Table 6.—Software Simulation Inputs

Input	Units	Value
Stages	-	1
Passes	-	1
Pump efficiency	%	80
No. vessels per stage		2
No. elements per vessel		1
System Recovery	%	15
Raw water flow	gpm	2.35
Feed flow	gpm	2.85
Concentrate flow	gpm	2.0
Concentrate recycle	gpm	0.5
Permeate flow	gpm	0.35
Membrane flux	gfd	9

The software simulations were conducted to determine the required feed pressure and the resulting permeate salinity for desalination of Well 3 water. The results of the ROSA simulations are shown in table 7.

Table 7.—Results of ROSA Simulations

Membrane	Feed pressure (psi)	Permeate TDS (mg/L)	Power (kW)	Specific energy (kWh/kgal)
BW30	104	32	0.16	7.7
XFRLE	81	32	0.13	6.0
LP	75	80	0.12	5.5
XLE	68	98	0.1	5.0
NF90	59	165	0.09	4.4

The results of the ROSA simulations determined that the BW30 membrane offers the highest salt rejection at the highest operating pressure, while the NF90 requires the lowest feed pressure; produces permeate with the lowest salt rejection, and

operates at the lowest specific energy. The NF90 membrane was chosen, because it offered the lowest operating pressure while still meeting the target water quality of < 500 mg/L TDS.

4.4 Data Collection and Analysis

For each experiment, information regarding the system configuration and orientation was recorded. Process conditions and experimental design considerations are shown in table 8. The GPS coordinates of the testing location were determined using mapping tools for use in the solar model calculations. System configuration information included pump, pump controller, membrane, and solar panel models. The orientation of the solar panels (both bearing and angle from horizon) was determined.

During testing, key operating parameters were recorded for each sampling event. Built-in rotameters were used to measure permeate and concentrate flow rates. A mass balance was used to calculate the feed flow rate. Pressure was measured using built-in gauges as indicated in figure 6 at the inlet and outlet of the cartridge filter and the feed to the first membrane element. Conductivity, pH, and temperature of all streams (i.e., feed, concentrate and permeate) were measured (Myron Ultrameter II-6PII). Panel surface temperature was measured using an infrared thermometer. Voltage and current from the PV panels and to the pump were measured manually with current clamps and a multimeter and simultaneously logged for further analysis. The solar irradiance was measured using a pyranometer (Apogee MP-200), and qualitative cloud conditions were noted. The pyranometer was mounted horizontally next to the panels about five (5) feet off the ground.

For the solar model calculations, solar zenith, panel incidence angle, and extraterrestrial solar irradiance were determined using the NREL Solar Position and Intensity calculator (SOLPOS) 2.0 model [NREL, 2000]. This model calculates the solar position relative to a panel given GPS coordinates, date, time, and panel orientation.

5. Case Study Results

5.1 Solar Model Case Study

The first objective of this project was to develop a performance metric that relates water production to the system's solar energy input. Since every solar-powered desalination system will be unique, it is imperative to develop a way of normalizing water production to develop a comparative metric that is influenced by as few system or operating characteristics as possible. While the goal is for this method to be extended to other solar-powered systems (e.g., solar distillation,

solar-powered EDR, microbial desalination, etc.), the PVRO system was used to initially develop the performance metric relating solar energy input to water production. The hypothesis was that given a system with consistent operating conditions, a single performance metric can be developed. Table 8 summarizes the variables that affect water production of a PVRO system and how they were either controlled or measured.

5.1.1 System Configuration and Testing Conditions

For this case study, the same system was used for all tests and the components are summarized in table 9.

With the same components, the PVRO system was operated on 3 days varying the geographic location and panel orientation (table 10). The first test was conducted at BGNDRF with the PV array oriented towards true south with an inclined angle of 36°. Test 2 was conducted with the same panel orientation but in Denver, Colorado (CO). The third test was conducted in Denver, CO, but the panel orientation was changed to a true east azimuth and 56° incline angle.

5.1.2 Feed Water and Operating Conditions

The water source for these tests was Well 3 groundwater from the BGNDRF. Standard water quality analysis was conducted to characterize inorganic composition, which is summarized in table 11. Trace metals were analyzed using inductively coupled plasma mass spectrometry (Environmental Protection Agency (EPA) method 6020A), and anions were measured using ion chromatography (EPA method 300). Alkalinity and TDS were quantified following Standard Method 2320 B and 2540 C, respectively. Silica analysis followed the HACH method 8185. According to the ROSA software, the osmotic pressure of this feed water was 23.7 pound per square inch (psig).

Table 8.—Performance Variables and Control Measures

Variable	Impacts	Controllable	Action
PV System Components	Conversion of solar energy to electrical energy	Yes	Use same PV panels and pump controller
Pump	Pumping efficiency	Yes	Use same pump. Calculate pump efficiency to confirm constant operation
Location	Solar energy input to system	Yes	Test at two locations Record GPS coordinates for test location Measure total irradiance with pyranometer
Panel Orientation	Solar energy input to system	Yes	Test with two different orientations Measure panel azimuth and incline angle Apply solar model to account for panel orientation
Membrane	Salt rejection and power requirements	Yes	Use same membrane for all tests Measure permeate conductivity and confirm consistent effluent quality
Water quality	Separation efficiency and fouling potential	Yes	Use same water quality Measure feed conductivity at each sampling event
Membrane Recovery	Permeate production per energy input	Yes	Adjust backpressure value to maintain constant recovery Measure permeate flow and conductivity to confirm consistent operation
Water Temperature	Membrane permeation	No	Measure water temperature with each sampling event
Ambient Conditions (temperature and wind speed)	PV panel efficiency	No	Measure PV panel temperature Collect weather data with ambient temperature and wind speed
Panel Cleanliness	PV panel efficiency	Yes	Clean panel before testing to remove dust

Table 9.—System Information for Summer 2015 PVRO Tests

Component	Brand/Model	Specifications
PV Panels	Grape Solar GS-S-100-TS	4 panels Total cell area: 2 m^2 Maximum power: 100 W per panel
Pump	Dankoff Solar Flow Pump 1304	1/5 hp, 24 VDC Max flow: ~8.1 L/min Max total dynamic head (TDH): ~140 psi
Pump Controller	Solar Converter, Inc Model: PPT 15 D 3R	Direct coupled PV to motor
Membrane	Dow Filmtec NF90-2540	Material: Polyamide thin-film composite

Table 10.—Summary of Test Variables for Solar Model Development

Test No.	Day	Location	Water	Panel Azimuth	Panel Angle
1	6/18/15	Alamogordo, NM	Well 3	True South	36°
2	6/24/15	Denver, CO	Well 3	True South	36°
3	6/25/15	Denver, CO	Well 3	True East	56°

Table 11.—Water Quality Analysis for Well 3 from BGNDRF
(All units are mg/L. Standard deviations are provided for replicate analyses.)

Parameter	Feed Water	Permeate	Concentrate
Barium	0.011 ± 0.003	Below detection limit (BDL)	0.015
Calcium	380 ± 3.7	5.03 ± .64	512
Magnesium	188 ± 2.9	2.21 ± 0.3	255
Potassium	3.21 ± 0.2	0.42 ± 0.025	4.26
Sodium	345 ± 5	40.4 ± 4.5	452
Strontium	6.74 ± 0.06	0.076 ± 0.009	9.09
Chloride	684 ± 12.3	68.4 ± 2.4	887 ± 12
Nitrate –N	2.8 ± 0.3	2.2 ±1.2	3.0 ± 0.03
Sulfate	1530 ± 17	17 ±8.4	2023 ± 25
Total Alkalinity as $CaCO_3$	193 ± 1.8	< 20	255 ± 4.6
Silica	9.6 ± 0.4	1.45 ± 0.63	16 ± 9
TDS	3263 ± 120	169 ± 30	4263 ± 235

During each of the three (3) tests, controllable operating conditions (i.e., water composition, recovery, and effluent water quality) were held as constant as possible. To confirm that the other operating parameters did not vary between tests, one (1)-way analysis of variance (ANOVA) tests were conducted.

The raw water conductivity was compared between test days as a proxy for changes in raw water quality. The average feed water conductivity between tests ranged from 4,311 to 4,378 µS/cm (table 12), which is a relative percent difference of 1.5 percent. The ANOVA analysis (figure A-1) found that the

variation between days was not significant at the 90 percent confidence level (probability (p) value =0.053).

Table 12.—Average Operating Conditions for Well 3 Case Study

Test No.	Feed Conductivity (µS/cm)	System Recovery	Permeate Conductivity (µS/cm)
1	4376 (± 87)	26.8% (± 2.8%)	341 (± 147)
2	4311 (± 77)	26.2% (± 1.5%)	339 (± 136)
3	4348 (± 58)	24.4% (± 2.7%)	305 (± 135)

For system recovery, the ANOVA analysis (figure A-2) found that at least one (1) of the three (3) operating days was statistically different (p=0.024). A Tukey comparison of means revealed that there was a statistical difference between test 1 (6-18 in NM) and test 3 (6-25 in CO). There was no statistical difference between tests 1 and 2, or tests 2 and 3. A Levene test determined that there is no significant difference in recovery variance between days (p=0.586). Despite differences, the average system recovery was within 2.4 percent between days.

For sampling events where the recovery was between 18 to 33 percent, the permeate conductivities were compared to determine if there was a variation in the effluent water quality. The conductivity varied with permeate production. Conductivities were higher at lower permeate fluxes (figure 9), which makes the ANOVA test on the whole data set less informative. When the permeate production was less than 1.25 L/min, there does appear to be systematic differences between test days with the NM south run producing permeate with systematically higher conductivities.

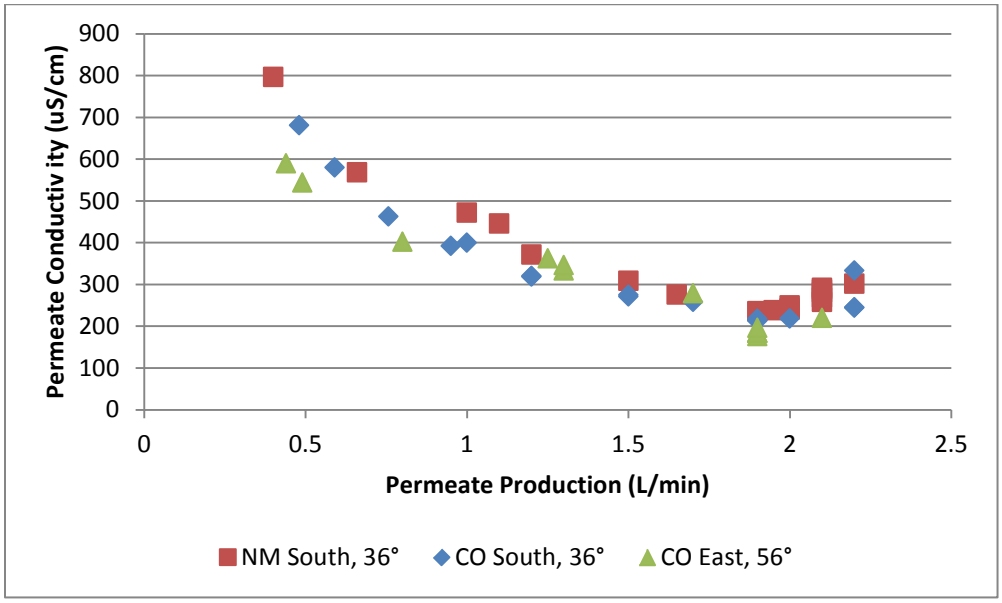

Figure 9.—Permeate conductivity as a function of permeate flow rate.

5.1.3 Evaluating Methods for Quantifying Solar Energy Input

The first step in developing a performance metric relating solar energy input to water production is to determine how to objectively quantify the solar energy input. Many models have been proposed with varying degrees of complexity to determine the irradiance on an inclined plane. Many empirical models focus on the determination of the direct and diffuse components given limited data. This section systematically tests assumptions regarding which solar model terms in an isotropic solar model are necessary to characterize the performance of a solar-powered water treatment system. The underlying driving force is to develop a characterization method that depends on a readily accessible measurement (GHI) and a technique accessible to water treatment engineers. The underlying assumption is that given the same treatment system, water quality, and operating conditions, there should be a constant relationship between energy input and water production. Model terms will be added incrementally to determine which components can be neglected to calculate the system performance efficiency.

5.1.3.1 Case 1—Global Horizontal Irradiance (GHI) Only

The first case considers the raw pyranometer readings as the sole metric for energy input to the system. Some studies report measuring GHI using a pyranometer but do not describe any additional modeling to quantify solar irradiance on the tilted solar collector [Kargar Sharif Abad et al., 2013; Sathyamurthy et al., 2015, 2014; Taghvaei et al., 2014]. This first case represents a basic, over simplified approach by comparing water production directly to the pyranometer GHI readings. This approach does not decompose the GHI into the direct and diffuse components, consider solar incidence angle or ground reflectance. Figure 10 shows that GHI had little variation over the three (3) test days. Only data points collected under full sun conditions are shown. The similarities, despite geographical location differences, may be due to a number of confounding effects. On a given day, GHI decreases with increasing latitude [Kreider and Kreith, 1981]. The CO test site (39.7222° N) is located further north than the NM test site (32.8839° N) suggesting the GHI readings in NM should be systematically higher, although not observed.

Altitude can affect GHI readings at the surface, but was not likely significant between the CO and NM test sites. The atmospheric path that radiation travels affects the net energy reaching the surface, which is quantified through the air mass. Air mass depends on the zenith angle and altitude. An air mass equal to 1 is defined as the path the sun travels when the zenith = 0 and at sea level. The CO test site was located at a slightly higher elevation (El 5612 ft) compared to the NM test site (El 4280 ft). Correcting for the relative differences in air mass between elevation differences follows Eqn 3, where m is the local air mass, m_0 is the air mass at sea level, p is the local pressure, and p_0 is the pressure at sea level. Given the measured differences in pressure between the two sites (1,021.6 hPa in

CO and 1,019.4 hPa in NM), the differences in local air mass was likely insignificant.

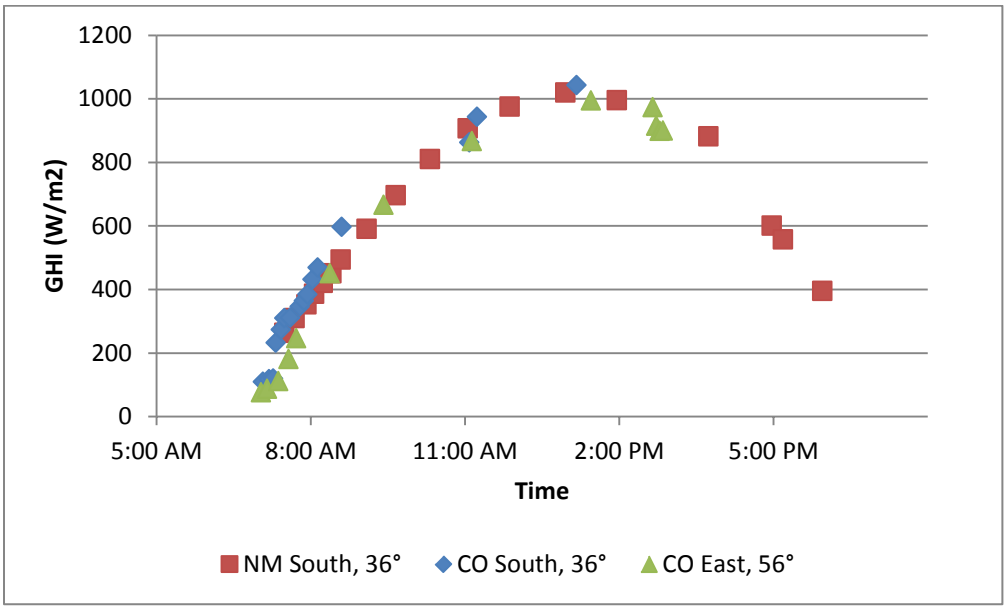

Figure 10.—GHI as a function of time for tests conducted on 3 different days.

$$m = \frac{p}{p_0} m_0 \qquad \text{Eqn 3}$$

Using GHI as a measure of energy input per unit area, the rate of energy input (W) can be computed by multiplying GHI by the total cell area of the panels (2 m^2). Figure 11 illustrates the relationship between energy input (GHI x Area) and permeate production for test 1 and reveals some important observations regarding system performance. At lower GHI levels, there is a linear relationship between GHI and permeate production. At higher GHI levels, there is a regime where permeate production is independent of GHI. This independence is due to the pump controller moderating the voltage sent to the pump to prevent over-speed.

If GHI were an adequate measure of energy input to the system, Figure 10 suggests that the permeate production in each of the three (3) tests should be the same for equal GHI values. Figure 12 demonstrates that GHI alone is not adequate for quantifying system performance. For similar GHI readings, the rate of permeate production differed significantly. Comparing the two (2) tests conducted with a south panel bearing and 36° tilt angle, the CO test produced systematically more water (~0.5 L/min) at the same rate of energy input. When the panel was oriented due east with a greater tilt (56°), the system produced more water per unit energy input early in the morning. In the afternoon when the solar incidence angle approached 90°, water production decreased even though GHI x Area exceeded 1,700 W. These results demonstrate that other geometrical

considerations need to be considered to generate a consistent performance metric independent of test location and panel orientation/bearing.

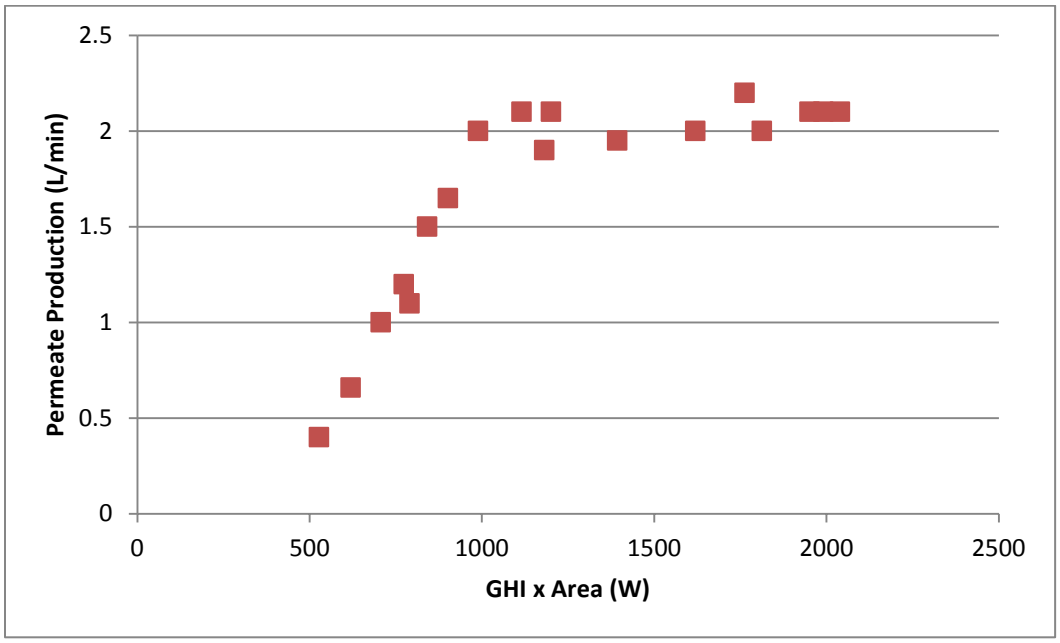

Figure 11.—Permeate production as a function of GHI for Test 1 (NM, south bearing, 36° tilt).

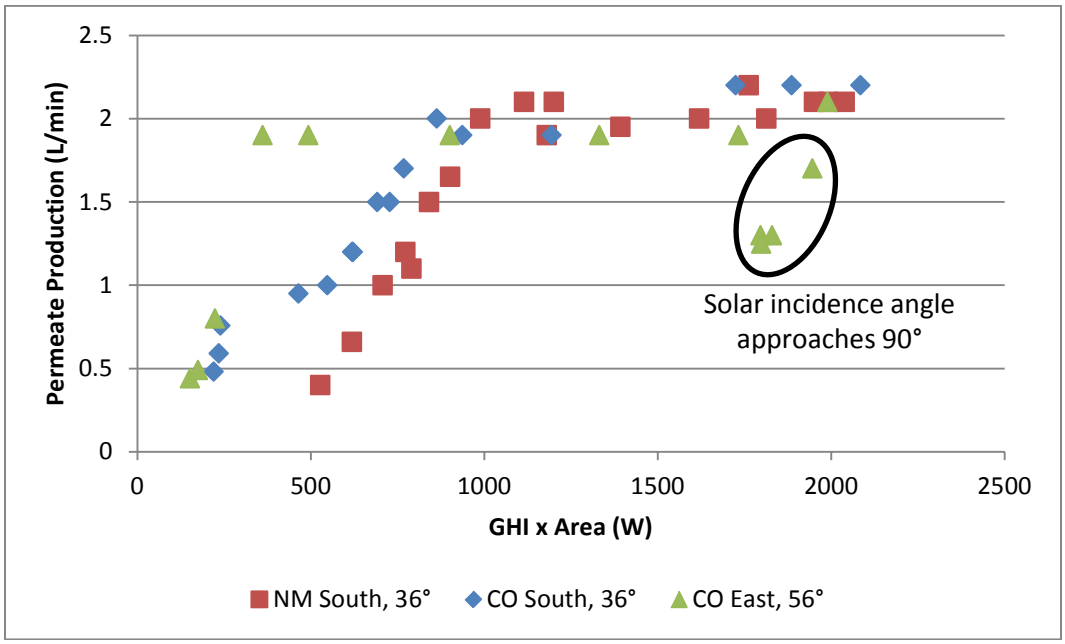

Figure 12.—Permeate production as a function of GHI x Area for Well 3 water tested at different locations (NM and CO), panel bearings (south and east) and tilt angles (36° and 56°)

5.1.3.2 Case 2—Isotropic Model with Direct Radiation, No Diffuse or Reflective

Solar radiation reaching a horizontal surface depends on the position of the sun in the sky (Z). When the sun is located directly overhead (small Z), a greater fraction of the total measured irradiance (GHI) stems from DNI compared to DHI. This case study quantified the energy input to the solar array by considering both the sun's position and panel orientation, but assumes that the contributions of diffuse radiation (DHI =0, DTI=0) and ground reflection (R=0) are negligible.

The derivation of this simplified model starts with Eqn 2 and assumes the DTI and R terms are both zero (Eqn 4). The direct radiation on the tilted panel (I_t) is a function of DNI and the angle of incidence (Eqn 5). DNI is not measured directly using the pyranometer but can be calculated based on Eqn 1. If diffuse radiation is assumed to be negligible, then the model simplifies to Eqn 6. Solving Eqn 6 for DNI (Eqn 7) and substituting back into Eqn 4 yields Eqn 8.

$$\boldsymbol{GTI = I_t} \quad \textbf{Eqn 4}$$

$$I_t = DNI \times \cos(\theta_i) \quad \textbf{Eqn 5}$$

$$GHI = DNI \cos(Z) \quad \textbf{Eqn 6}$$

$$DNI = \frac{GHI}{\cos(Z)} \quad \textbf{Eqn 7}$$

$$GTI = I_t = \frac{GHI}{\cos(Z)} \cos(\theta_i) \quad \textbf{Eqn 8}$$

The Z and $\cos(\theta_i)$ angles in 1 minute increments were calculated using the SOLPOS model (NREL, 2000) given the latitude and longitude coordinates for the two (2) sites. Between the NM and CO test sites there were small variations in the Z angle (figure 13). In the early hours just after sunrise, the zenith in NM was greater than CO, and the cos(Z) term will be small, thus, inflating the calculated GTI in NM. At solar noon, the zenith in CO is greater having a similar inflationary effect.

There were greater systematic differences in θ_i between the two (2) sites (figure 14). When both panels were oriented towards true south and tilted 36° from horizontal, $\cos(\theta_i)$ was systematically greater at the CO location due to the greater latitude. Based on Eqn 8, a larger $\cos(\theta_i)$ will inflate the calculated GTI leading to more water produced per unit energy input. When the panel was oriented true east, $\cos(\theta_i)$ is greater earlier in the day because the panel normal vector is pointed towards the sun. The calculated GTI as a function of time shows that these differences in $\cos(\theta_i)$ for the panel with an east bearing have a large effect on incident solar radiation (figure 15). For the east oriented panel, the GTI is greater earlier in the day compared to the southern facing panels.

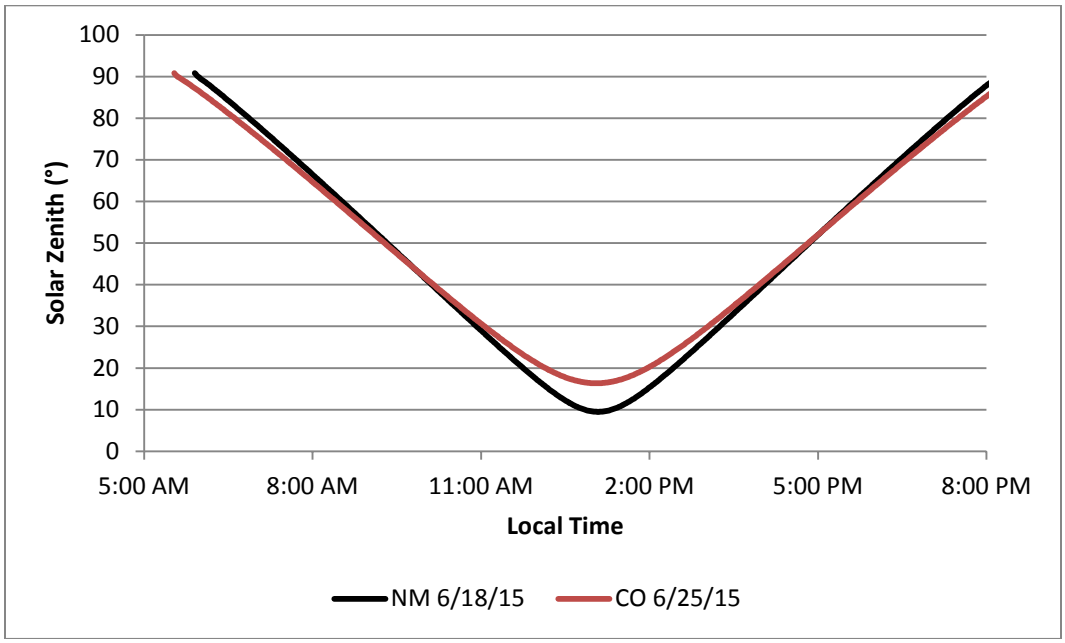

Figure 13.—Solar zenith angle as a function of local time for NM and CO test sites.

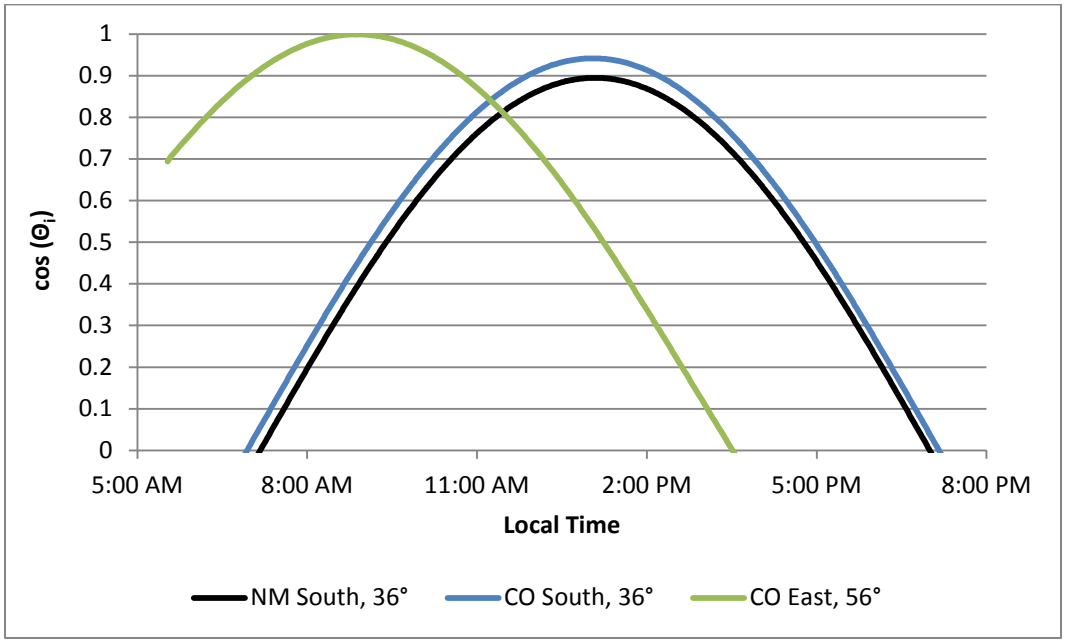

Figure 14.—Cosine of the solar incidence angle on panel as a function of local time for the three tests.

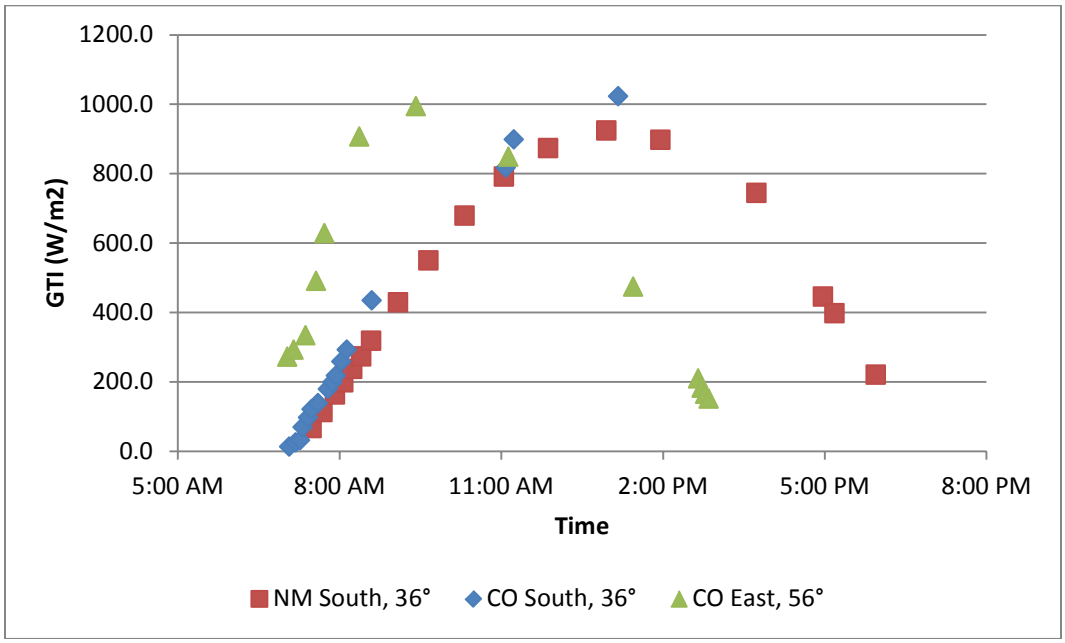

Figure 15.—Irradiance on a tilted surface following an isotropic model neglecting the diffuse and reflection terms for the three different test conditions.

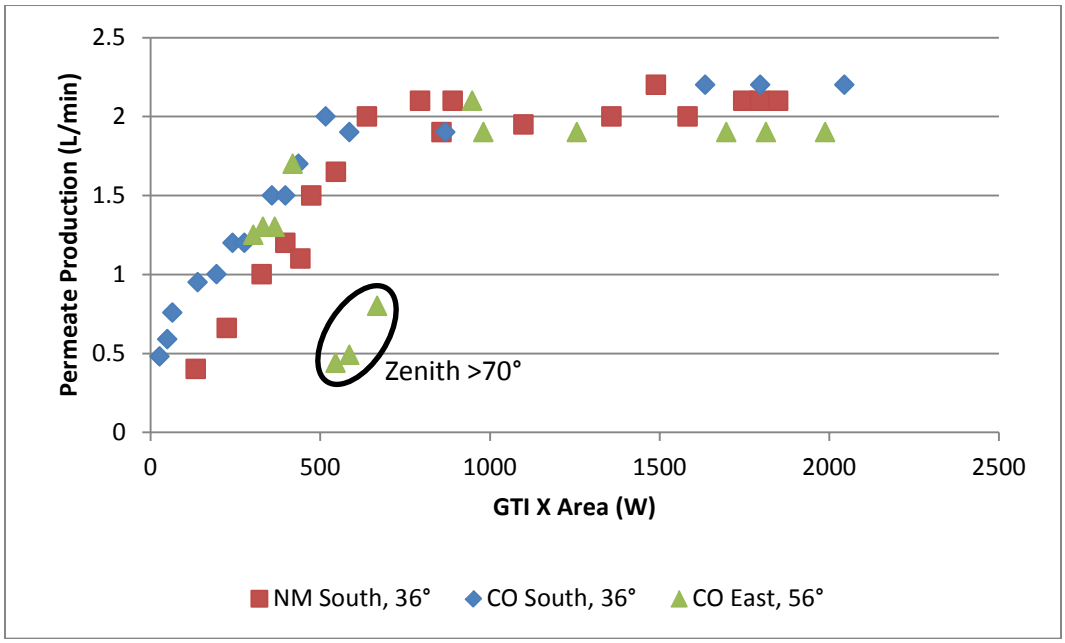

Figure 16.—Rate of permeate production as a function energy input for an isotropic model considering only direct radiation (diffuse and reflection is negligible).

Using the direct-only GTI values as a measure of solar input produced a more consistent performance metric between the rates of energy input and permeate production (figure 16). For the CO south test, the low energy input data points conform better to the rest of the data set and do not appear offset as in figure 12. The CO east data points with a permeate production between 1.25-1.75 L/min

agree with the other tests; the GTI calculation adequately corrected for the large solar incidence angle decreasing the incident irradiance. For the same test, the data points collected early in the morning with Z greater than 70° do not agree with the other tests. The GTI appears to be overestimated under the direct radiation-only model assumptions. This deviation is expected as it is unreasonable to neglect diffuse radiation at high Z angles where the air mass and scattering is greater.

This approach of quantifying the solar irradiance on the tilted panel only considered the direct radiation component and neglecting diffuse or reflected radiation. While this method is greatly improved over using measured GHI values, it does not account for times when diffuse radiation is dominant, and Z is approaching 90°.

5.1.3.3 Case 3—Isotropic Model with Direct and Diffuse Radiation, No Reflectance

To improve over the simplified model in Case 2, Case 3 includes both the direct and diffuse radiation components, but neglects reflective radiation off the surrounding ground. Revisiting Eqn 1, GHI is comprised of both DNI and DHI components. Several empirical models have been developed to estimate the relative magnitude of the DNI and DHI components based on only a GHI measurement.

$$GHI = DNI\ cosZ + DHI \qquad \textbf{Eqn 1}$$

Many empirical models are based on the premise that the Total Clearness Index (Kt) provides an indication of the relative contribution of diffuse radiation (DHI) to the global irradiance (GHI). Kt is calculated according to Eqn 9, where I_0 is the Extraterrestrial Radiation (W/m^2), and Z is the zenith. I_0 varies throughout the year but is practically constant over the course of a day. The value of I_0 was estimated using the SOLPOS model.

$$Kt = \frac{GHI}{I_0 cos(Z)} \qquad \textbf{Eqn 9}$$

Two empirical models tested in this study use the Kt value in a piecewise relationship to estimate the ratio of DHI/GHI. The piecewise regressions are presented in table 13 for both the Orgill and Hollands correlation and the Erbs correlation. The Orgill and Hollands correlations was developed over 4 years in Canada [Orgill and Hollands, 1977]. Alternatively, the Erbs correlation was developed at lower latitudes in the United States [Erbs, Klein, and Duffie, 1982]. Despite the geographical differences and the differences in Kt bins used, both models predicted DHI/GHI ratios in good agreement with each other when

applied to this data set. The Orgill and Hollands correlation systematically predicted a slightly greater value at low DHI/GHI ratios (figure 17).

Table 13.—Empirical models to estimating DHI/GHI from Meyers 2013.

Correlation	Relationship	Kt Bin
Orgill and Hollands Correlation	DHI/GHI = 0.177	Kt>0.75
	DHI/GHI = 1.577 – 1.84 Kt	0.35≤ Kt ≤ 0.75
	DHI/GHI = 1.0 – 0.249 Kt	0 ≤ Kt < 0.35
Erbs Correlation	DHI/GHI = 0.165	Kt > 0.80
	DHI/GHI = 0.951 – 0.160 Kt + 4.388 Kt^2 – 16.64 Kt^3 + 12.34 Kt^4	0.22 ≤ Kt ≤ 0.80
	DHI/GHI = 1.0 – 0.09 Kt	0 ≤ Kt < 0.22

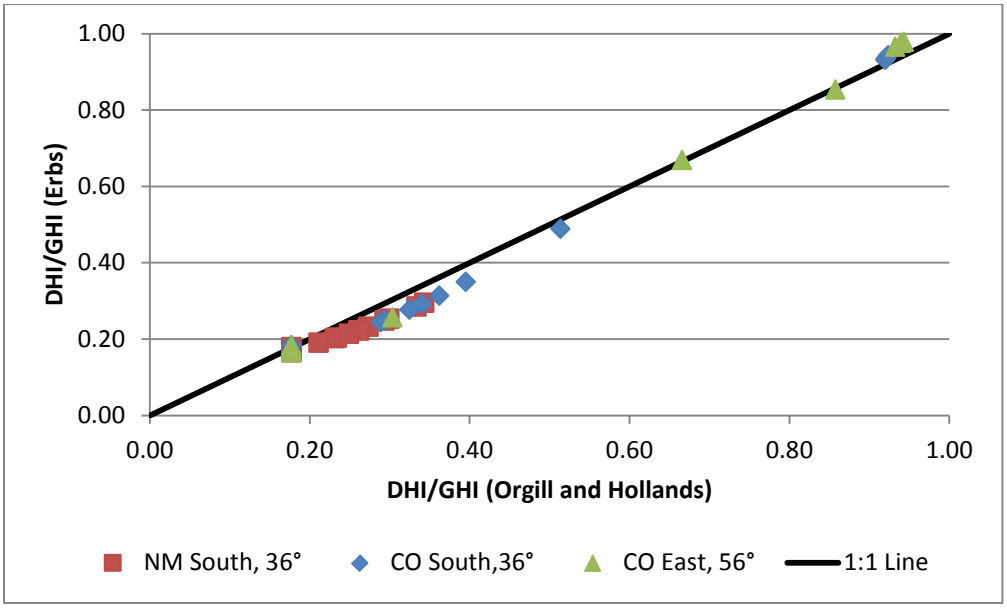

Figure 17.—Comparison of DHI/GHI ratios from the Orgill and Hollands correlation compared to the Erbs correlation.

Once the ratio of DHI to GHI is calculated, the pyranometer GHI measurements were used to determine the diffuse component (DHI). Eqn 1 was applied to solve for DNI using the solar zenith calculated from the SOLPOS model. Lastly, the total irradiance on a tilted plane (GTI) is determined following Eqn 10, which defines GTI as the sum of both the direct and diffuse components. The direct irradiance on the tilted plane is calculated following Eqn 11, and the diffuse component is determined following Eqn 12 [Kreider and Kreith, 1981; Myers, 2013]. Despite differences in the DHI/GHI ratio from the two empirical models, the total energy input (GTI x cell area) were in good agreement with each other (figure 18). While there was little difference in the two correlations, the Erbs Correlation was used moving forward since it was developed at a latitude more representative of the test sites.

$$\boldsymbol{GTI = I_t + DTI} \qquad \textbf{Eqn 10}$$

$$I_t = \frac{GHI - DHI}{\cos(Z)} \cos(\theta_i) \qquad \textbf{Eqn 11}$$

$$DTI = 0.5\, DHI\, (1 - cos(\beta)) \qquad \textbf{Eqn 12}$$

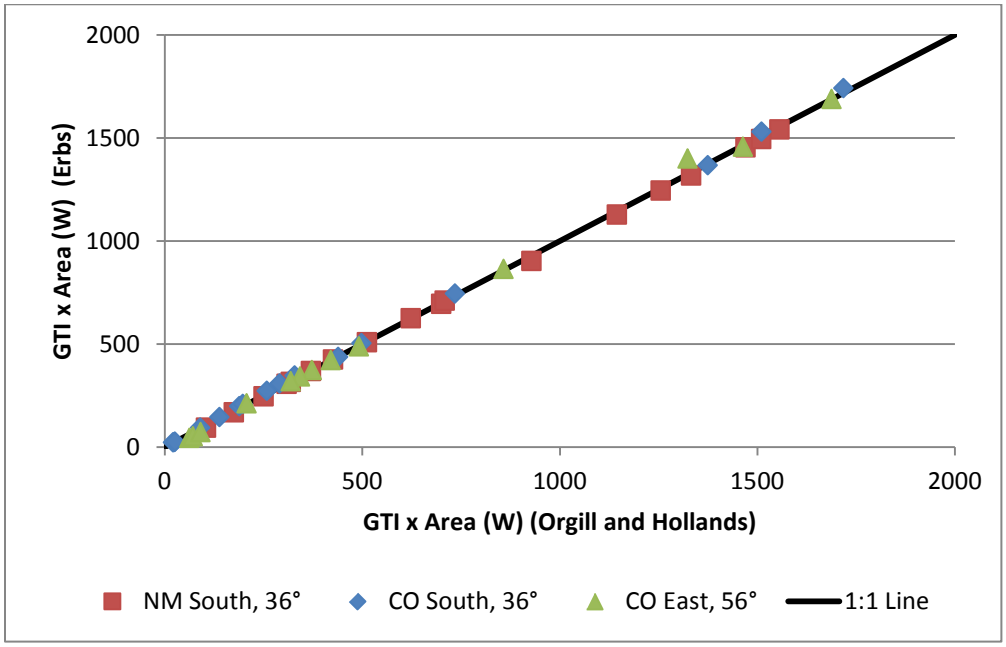

Figure 18.—Comparison of energy input rate (W) for the Erbs and Orgill and Hollands Models. Solid line indicated 1:1 line.

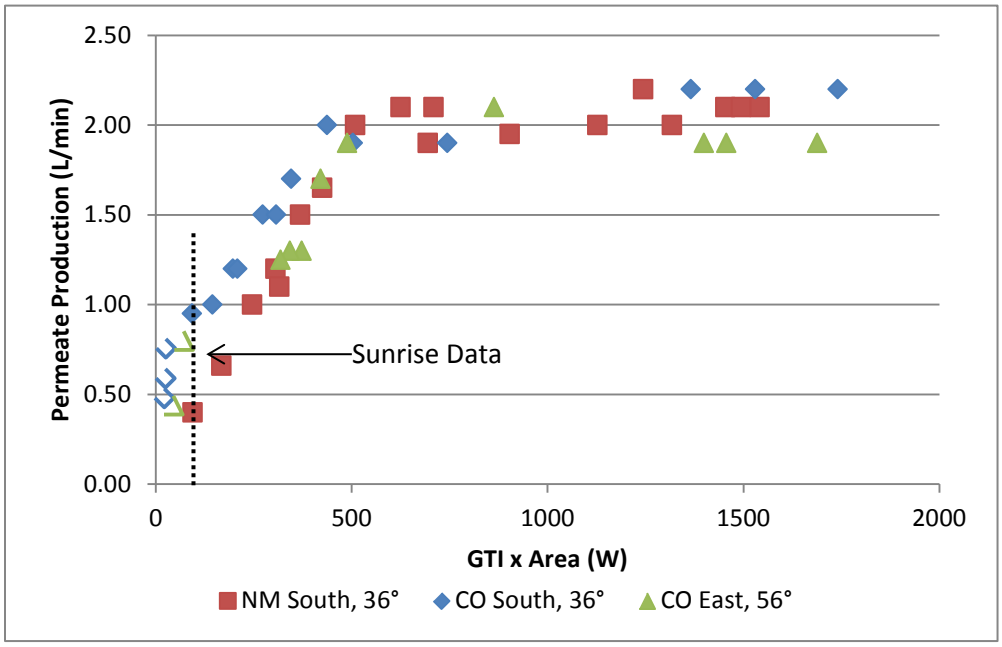

Figure 19.—Rate of permeate production as a function energy input for an isotropic model considering direct and diffuse radiation (reflection is negligible). Measurements at sunrise with clouds indicated by unfilled markers.

Plotting the solar energy input as a function of permeate production shows an improvement over Case 2 (direct only model, figure 17). Most noticeable is the lack of systematic outliers from the CO east test at high Z angles. Between the three (3) tests, the energy input threshold where the system reaches full production capacity is consistent around 500 W. There still appears to be systematic difference between the CO south test and the other two (2) tests, which suggests there is an unaccounted variable affecting permeate production. Measurements taken at sunrise when clouds were present (unfilled markers, figure 19) indicate increased scatter compared to the rest of the curve.

5.1.3.4 Case 4—Isotropic Model with Direct, Diffuse, and Reflectance

One factor that may have contributed to the systematic differences in figure 19 is the neglecting of any reflective radiation inputs. Both direct beam and diffuse radiation can reflect off the ground surface and contribute to the total solar irradiance on the tilted surface. The testing location in NM was surrounded by a combination of concrete and gravel. The CO testing location was conducted on asphalt. The fraction of radiation that a surface reflects is quantified by the surface albedo. According to table 14, the albedo at the CO test site may be systematically lower (worn asphalt) compared to the NM site.

Table 14.—Tabulated Albedo Values for Surfaces Present at Test Sites from Various Sources [Deutsche Gesellschaft für Sonnenenergie, 2008; Pisello, Pignatta, Castaldo, & Cotana, 2014; Santamouris, 2013].

Surface	Typical Albedo
Concrete	0.30
Gravel	0.18-0.72, 0.2-0.4
Asphalt	0.1-0.2 (0.2 if worn)

To determine the effect of reflective radiation on the solar energy input model, the reflective terms were added to the GTI calculation assuming an albedo (ρ) of 0.2 at the CO location and 0.3 at the NM site. To incorporate the ground R into the solar irradiance calculations, the equation for GTI has an additional term shown in Eqn 13.

$$\boldsymbol{GTI = I_t + DTI + 0.5\rho(1 - cos(\beta))(DNI + DHI)} \qquad \textbf{Eqn 13}$$

Including the reflection terms caused a systematic increase in the calculated power input at all input levels (figure 20). Comparing the NM south and CO south tests with the same panel bearing and angle, the GTI increase was greater for NM south due to the higher surface albedo. For the CO east test with the greater tilt angle, the reflection term increased the GTI estimate more, confirming the greater reflection contribution at higher tilt angles.

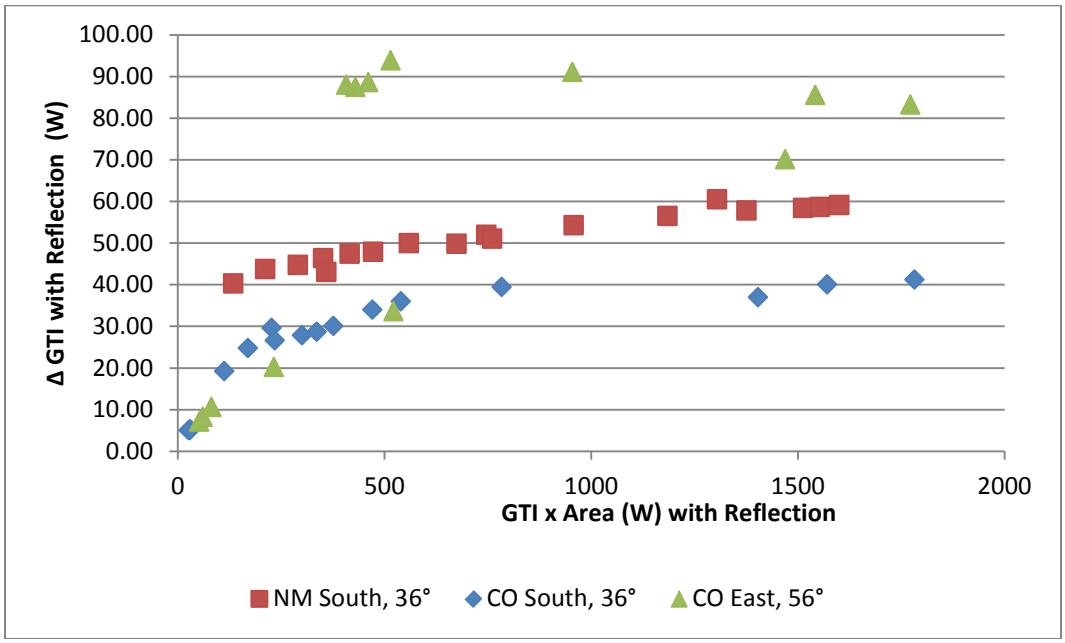

Figure 20.—Change in GTI estimation with the inclusion of the reflection term as a function of calculated power input

A reflection estimate had no practical effect on normalizing the performance metric between the CO south and NM south tests. Compared to Case 3 (no reflectance), more uncertainty (scatter) was observed for the CO east test (figure 21). These results suggest that neglecting the reflective term is not the source of the systematic differences between tests, and including this term may introduce more error without a proper albedo measurement for the surrounding surface.

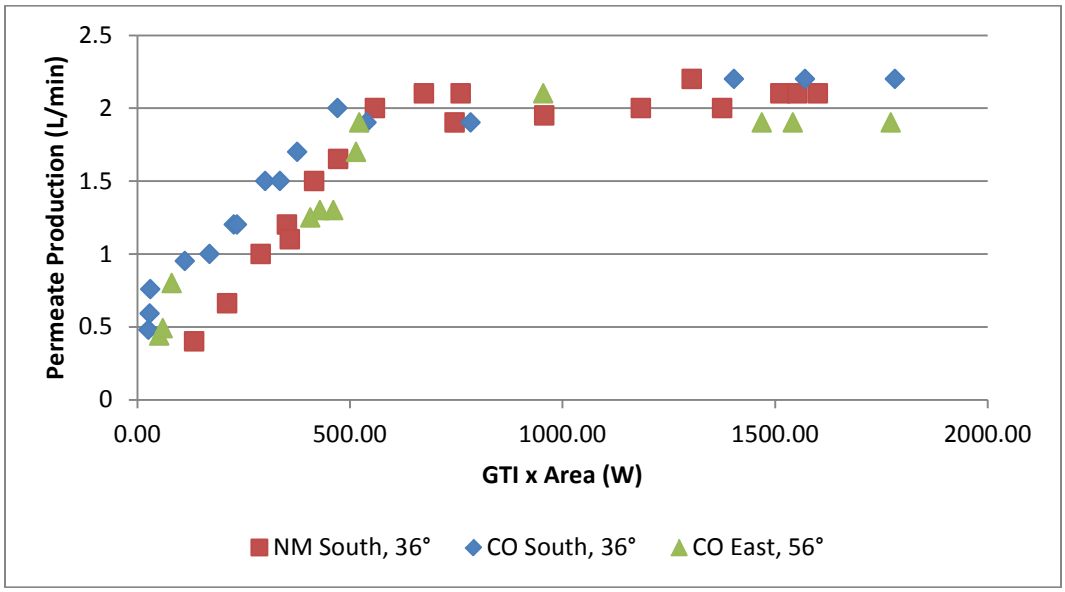

Figure 20.—Rate of permeate production as a function energy input for an isotropic model considering direct, diffuse, and reflective radiation.

5.1.3.5 Case 5—Cloud Event

The last aspect investigated in applying the isotropic model was the case of a cloud event. During the Test 2, there was a cloud event mid-morning when an isolated cloud passed in front of the sun over the course of 10 minutes, as indicated in figure A-7a. During this time, the pyranometer reading and permeate flow was recorded in rapid succession. Another cloud event occurred during Test 3 as illustrated in figure A-7b. Inspection of the discrete power measurements compared to the real-time power data from the data logger revealed that this measurement occurred at a very dynamic period. The discrete voltage and amperage readings did not agree well with the logged data. Therefore, this data point has increased uncertainty relative to others.

When the isotropic model with direct and diffuse terms is applied to these data, they appear as outliers compared to data collected under clear skies (figure 22). In each case, the isotropic model underestimates the energy input. It was not expected that the isotropic solar model would be able to accurately account for the solar irradiance on the plane. A large body of work has been conducted determining the decrease in GHI due to clouds depending on fractional cloud cover (i.e., octa) and Z [Myers, 2013]. Octa is a unit of measure that estimates cloud coverage by diving the sky into eighths (8ths) an quantifies how many sections are obscured by clouds. To estimate the irradiance on a tilted surface, the

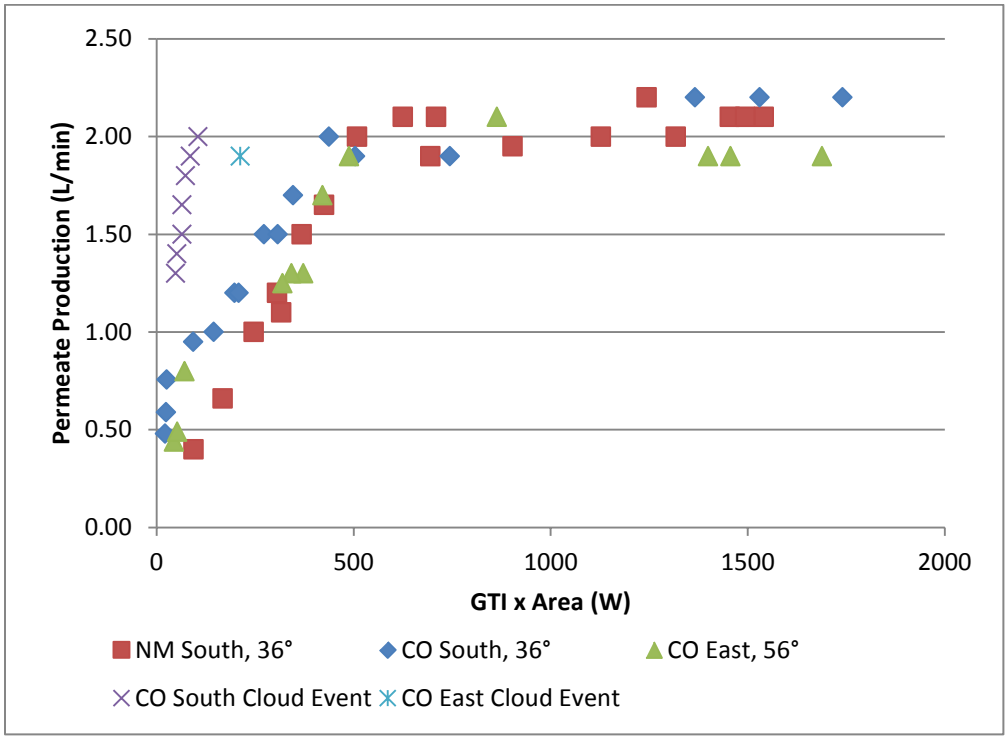

Figure 21.—Rate of permeate production as a function energy input for an isotropic model considering direct and diffuse including cloud events.

position of the clouds relative to the panel face is another important variable that is difficult to model empirically. In this case, a more accurate method to determining GTI under varying sky conditions would likely be mounting a pyranometer at the same angle as the solar collector. A promising conclusion is that in these cases, the water production was greater than expected given the measured GHI.

5.1.3.6 Solar Model Lessons and Recommendations

The primary purpose of the Solar Model case study was to investigate the use of an isotropic solar model to estimate solar irradiance on a PV panel array in an effort to relate the rate of energy input to the rate of water production. Increasingly complex models were considered to determine the feasibility of developing a metric to evaluate system performance. Including both the direct and diffuse terms yielded best normalization between tests. The addition of a reflectance term adds complexity, assumptions, and showed no sign of improving the relationship. There are likely several factors influencing the uncertainty (scatter) observed in figure 19.

First, the rotameter used to quantify permeate flow has rather poor resolution (0.25 L/min increments) that is susceptible to measurement reading error. There may be bias between operators taking the measurement, which may influence the performance metric. A digital rotameter would help minimize this uncertainty.

The pyranometer has uncertainty approaching ±10 percent at small solar elevations, which correspond to early morning and late afternoon measurements [Myers, 2013]. Most of the measurements that fall on the line where permeate production depends on GTI x Area are recorded in the early morning when instrument uncertainty is greatest. At times when the zenith is smaller and the instrument likely more accurate, the system was operating at full capacity.

There is inherent error in the isotropic solar model. Case 2 demonstrated that failure to decompose the direct and diffuse radiation components leads to a poor relationship between calculated irradiance and permeate production. Decomposition into the different components is based on empirical models, which have inherent uncertainty. Additionally, many data points used in developing the metric were collected during low solar elevations where proper estimation of the diffuse component is important. According to Myers [2013], calculations of direct beam irradiance commonly have 10 to 15 percent uncertainty. Accuracy of the isotropic model can be improved by using a shadow band on a second pyranometer that would measure the diffuse component directly, eliminating the need for empirical models. Beyond the isotropic model, there are anisotropic models and models that consider atmospheric turbidity that may better account for observed differences. Moving away from modeling, a pyranometer mounted at the same angle of the panel array would directly measure the irradiance on the PV

array, including direct, diffuse and reflective components [Myers, 2013]. This simple modification would eliminate most of uncertainty associated with modeling assumptions and may be operationally easier than investigating more complex modeling approaches.

5.1.3.7 Multilinear Regression Modeling

Adding terms to the isotropic solar irradiance model did not fully correct for the systematic differences between tests. Figure 19 shows that even with the same panel bearing and orientation, the CO south test produced more water for the same solar irradiance compared to the NM south test. These results suggest that there is another factor affecting the water production rate that cannot be accounted for by the solar irradiance estimation alone. Other potential factors include the PV panel temperature, permeate water quality, and water temperature. PV panel efficiency is inversely related to panel temperature [Skoplaki and Palyvos, 2009]. Flux through the membrane increases with water temperature [American Water Works Association, 2010].

The manufacturer supplied temperature correction factors for this membrane were applied to normalize the permeate production due to temporal changes in permeate temperature throughout the day. Permeate temperature increased about 10°C over the course of the testing period for each day with systematically lower temperatures during the CO east test (figure A- 8). Normalizing the permeate production for the different water temperatures did not correct for systematic differences observed during testing (figure A- 9). Therefore, there is another factor affecting permeate production besides solar energy input and water temperature.

Multilinear regressions were investigated to determine which additional variables have an effect on permeate production. Only the data where the solar irradiance (GTI x Area) less than 500 W was used in an attempt to identify the discrepancies observed when the system is operating below full capacity. Solar irradiance (Irr), PV panel temperature (T_{Panel}), permeate temperature (T_{Perm}), permeate conductivity ($Cond_{Perm}$), recovery (Rec), and rejection (Rej) were screened for significance in the form of Eqn 14. The solar irradiance input used was the modeled GTI x Area from the isotropic model including both direct and diffuse components (Case 3). Given the different units of measures, all inputs were normalized to a mean of 0 and standard deviation of 1 prior to model fitting.

$$\boldsymbol{Q = Const + A * Irr + B * T_{Panel} + C * T_{Perm} + D * Cond_{Perm} + E * Rej + F * Rec} \qquad \textbf{Eqn 14}$$

An initial stepwise screening determined that the recovery and panel temperature are not a significant model terms (p=0.846 and p=0.842, respectively). The panel temperature finding is consistent with the manufacturer specifications for the panels that reported that a 1°C change in panel temperature decreases the

maximum power by only 0.38 percent. During these sampling events, panel temperature ranged from 14-36°C. Upon removing these terms, models with the Irr and T_{Perm} terms with either the $Cond_{Perm}$ or Rec terms were significant. If both the $Cond_{Perm}$ and Rec terms were included, then the Rec term was found to be insignificant (p=0.596) likely due to collinearity. The best-fit model included only the $Cond_{Perm}$ term (R^2_{adj} = 0.941). Comparing the normalized effects reveal some trends (Figure 15). As expected, an increase in solar irradiance increased permeate production. On the other hand, increases in both permeate temperature and conductivity decreases permeate production. The sign of the T_{Perm} term is not intuitive. Membranes are supposed to generate more permeate at higher temperatures. The inverse relationship between permeate production and permeate conductivity adheres with the standard observation that Rej (hence permeate conductivity) is inversely related to flux (figure 9).

Table 15.—Normalized Main Effects for Multilinear Regression Modeling Permeate Production as a Function of Solar Irradiance, Permeate Temperature, and Permeate Conductivity

Term	Normalized Effect	p-Value
Constant	1.169	<0.001
Irr	0.336	<0.001
T_{Perm}	-0.115	0.001
$Cond_{Perm}$	-0.218	<0.001

R^2_{adj}=0.941
R^2_{pred}=0.918

Models including interaction terms were investigated. While the individual terms were found to be significant (p<0.01), the R^2_{pred} diagnostic metric decreased suggesting overfitting. There are likely too few data points and too much correlation between uncontrollable variables to adequately investigate higher order models. Converting the model back to native units yields Eqn 15 with the units specified.

$$\boldsymbol{Q = 1.93 + 0.0019(Irr) - 0.031(T_{Perm}) - 0.0014(Cond_{Perm})}$$

With the following units

Q: [L/min]
Irr: [W]
T_{Perm}: [°C]
$Cond_{Perm}$: [µS/cm]

Eqn 15

Despite best efforts to consistently operate the system over multiple testing days, there were enough systematic variations in the permeate conductivity and temperature to affect the measured permeate flow rate. Therefore, metrics that relate solar energy input to permeate product either need to be adjusted for other operational parameters or be kept within the context that other parameters affect the acceptable uncertainty.

5.1.3.8 Proposed System Operating Curve

Examining all the data in figure 19 as a whole suggests that this system has a unique operating curve that relates solar energy input to permeate production. Given a rate of solar energy input, the permeate flow rate can be calculated. The curve has two operating regimes: one where permeate depends on solar input and one where the system is operating at full capacity (figure 23).

Regressions were fit to each regime to determine a piecewise relationship that predicts permeate flow as a function of solar energy input. When the system is operating below capacity, a linear relationship relates permeate production to energy input. The 95 percent confidence interval on the slope parameter is ±20 percent. For the prediction of new observations, the 95 percent prediction interval is ±0.4 L/min. In the full capacity regime, flow is constant and equal to 2.0 with a 95 percent confidence interval of ±0.05 L/min.

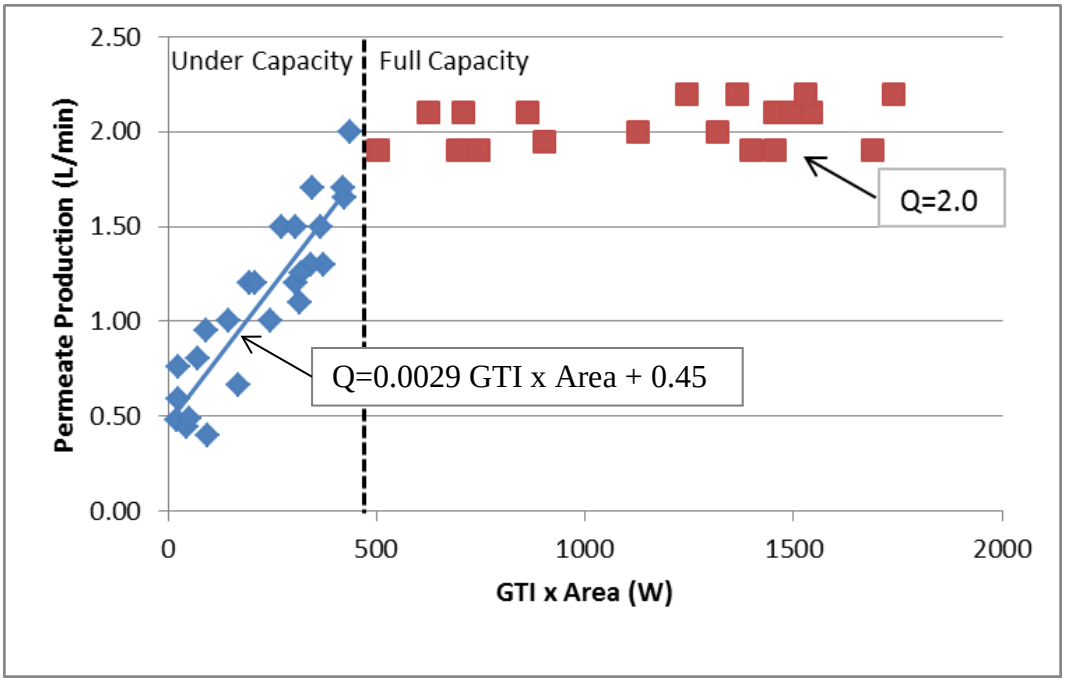

Figure 22.—Operating curve for PVRO system operating with BGNDRF Well 3 water at ~25 percent recovery.

This approach of characterizing a solar-powered system with the proposed operating characteristic curve is different from how PVRO systems are typically characterized. Most studies will measure the total energy generated by the PV panels (i.e., kWh) and compare it to the total water produced (i.e., m^3 permeate). This approach may suffice for simple PVRO systems, but it is not valid when other uses of solar energy are employed that do not generate electrical energy. This approach of estimating solar energy input based on system geometry and

orientation also forces the reporting of important system parameters (e.g., panel azimuth and angle) that are so often neglected but necessary to compare different solar-powered technologies. The proposed tool allows users to predict water production given any solar energy profile between different locations and quantitatively vet the effect that system upgrades have on performance in a manner that is more detailed than reporting a bulk kWh/m^3, which may not capture all uses of solar energy.

Identifying the operating regimes of a given system also provides a quantitative tool for predicting water production given a system-specific operating curve. Figure 24 provides a hypothetical, illustrative example. Given the solar input (GTI x Area) of a particular location (angle and bearing), the water production as a function of time can be calculated. Comparing figure 24a and figure 24b, the scenario in part "a" has a much greater solar input across the day compared to the scenario in part "b." These differences could be attributed to difference in system geographic location, time of year, or panel orientation. In scenario b, the system still reaches full capacity but would have lower water production in the early and late part of the day. By integrating the area under the curve, the total expected water production could be predicted.

5.2 Water Quality and Recovery Case Study

The characteristic operating curve developed in section 5.1 was based on the same water quality from the BGNDRF site. In this case study, the effect of water quality and recovery is evaluated by comparing the data from the Well 3 water to synthetic water with a different water quality. It is hypothesized that the water quality and operating recovery will have an effect on the relationship between solar energy input and water production.

5.2.1 System Configuration and Testing Conditions

The PVRO system used was identical to the system described in section 5.1.1 and system components are specified in table 9. This test was conducted at BGNDRF using the testing conditions listed in table 16.

5.2.2 Feed Water and Operating Conditions

This test was conducted using a synthetic solution with 2 g/L NaCl added to RO permeate. According to ROSA, the osmotic pressure of this water was 26.2 psig, which is 2.5 psig higher than Well 3 water. Compared to Well 3 water that contains significant calcium sulfate, this solution has a lower propensity to foul the membrane. The target recovery was 30 percent, but recovery increased steadily overtime (figure 25). Over the course of the testing period, the feed

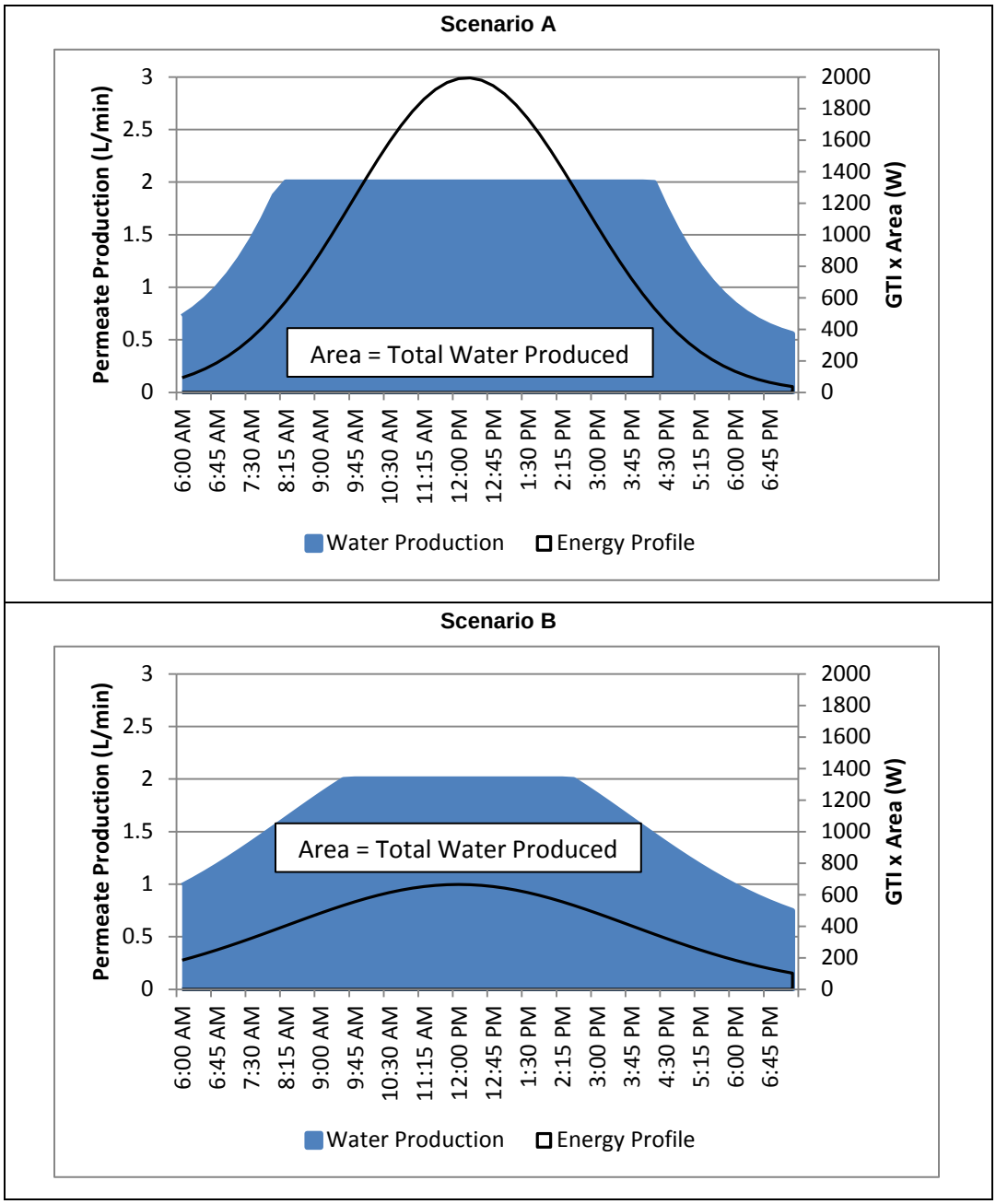

Figure 23.—Two hypothetical scenarios calculating the water produced for two different solar input profiles given this systems operating curve.

Table 16.—Summary of Test Variables for Model Development

Test No.	Day	Location	Water	Panel Azimuth	Panel Angle
1	6/18/2015	Alamogordo, NM	Well 3	True South	36
2	6/24/2015	Denver, CO	Well 3	True South	36
3	6/25/2015	Denver, CO	Well 3	True East	56
4	6/17/2015	Alamogordo, NM	2 g/L NaCl	True South	36°

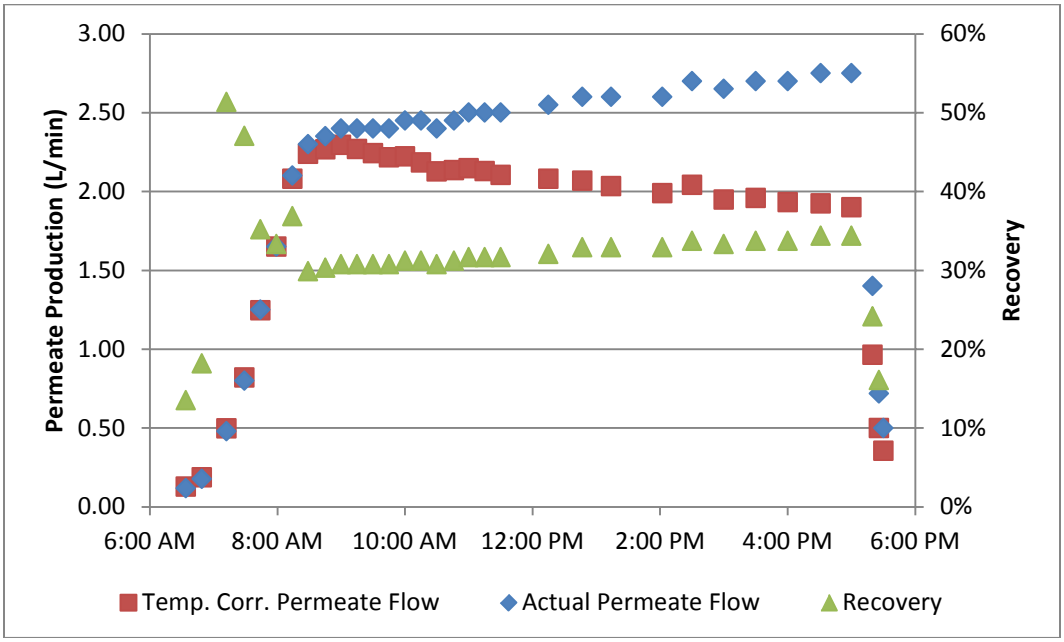

Figure 24.—Permeate flux and recovery over the testing period.

conductivity was constant at 3,797 ± 81 µS/cm. Similar to the Well 3 tests, permeate conductivity decreased with increasing flux. Operating at full capacity, the permeate conductivity was 389 ± 4 µS/cm, representing a NaCl rejection of 90 percent.

Table 17.—Water Quality Analysis for NaCl Synthetic Water
(All units are mg/L)

Parameter	Feed Water	Permeate	Concentrate
Barium	<0.003	<0.003	<0.003
Calcium	2.16	0.37	2.91
Magnesium	1.04	0.15	1.42
Potassium	1.52	0.15	2.0
Sodium	739	74	1050
Strontium	0.034	0.0049	0.047
Chloride	1130	118	1740
Nitrate –N	1.3	1.06	1.5
Sulfate	13.5	2.05	18.3
Total Alkalinity as $CaCO_3$	< 20	< 20	< 20
Silica	1.22	< 1	1.25
TDS	2260	215	2850

Permeate flow increased rapidly until about 8:30 am, after which point the flow started to level off (figure25). Unlike the Well 3 tests, flow increased steadily through 5:00 pm rather than remain constant. Manufacturer supplied permeate

correction factors were applied to determine if the increasing flux was due to increasing permeate temperature. Temperature normalized permeate production decreased over time indicating that temperature is not the only factor affecting permeate production. Feed pressure was not correlated with the change in flux, suggesting that the observed trend in flux is not related to the pump performance. Chronologically, this test with NaCl was conducted with a new membrane prior to the Well 3 tests. The system was operated for several hours the previous day, but the membrane may not have reached full compaction or steady state flux prior to this test.

5.2.3 Evaluation of Water Quality and Recovery Effect

The isotropic solar model including both direct and diffuse terms (section 5.1.3.3) was applied to the measured pyranometer readings to develop a characteristic operating curve for this test. Figure 26 compares the relationship between solar energy input (GTI x Area) to permeate production for both the Well 3 tests and the 2 g/L NaCl test. For a given energy input, the NaCl test systematically produced more water. Some hysteresis is apparent in the NaCl test where the afternoon permeate production was greater than the morning production at a similar energy input due to increasing recovery. This difference is attributed to unsteady state membrane transport properties.

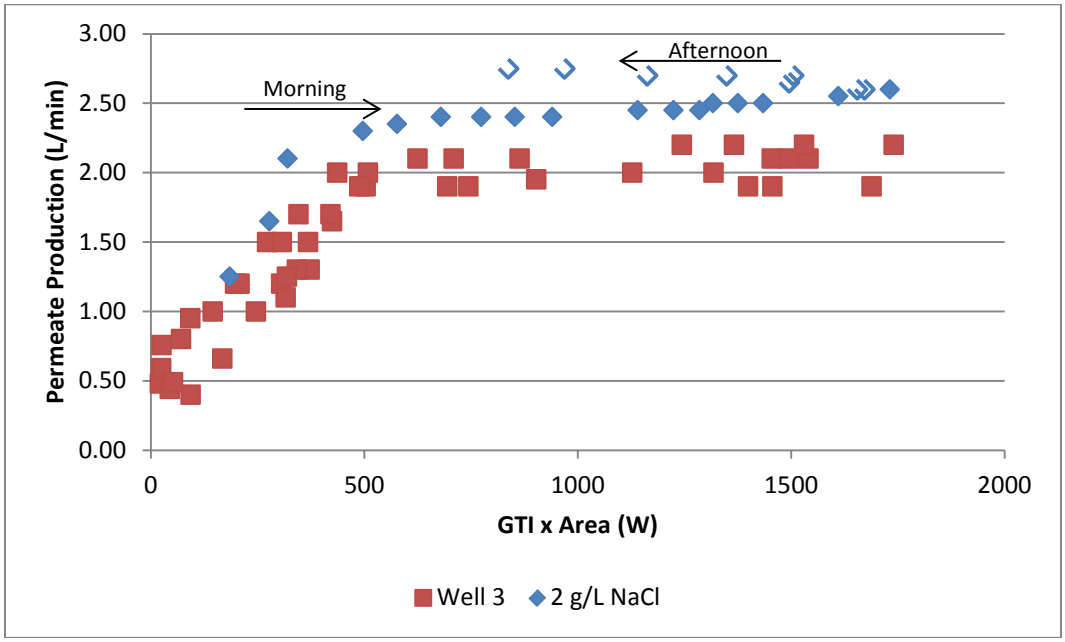

Figure 25.—Operating curve for PVRO system operating with BGNDRF Well 3 water at ~25 percent recovery and 2 g/L NaCl at ~32 percent recovery. For the NaCl test, samples collected during the afternoon have unfilled markers.

It is difficult to compare the Well 3 and NaCl tests directly in terms of the operating curve as both the feed osmotic pressures and recoveries differed. The NaCl test operated with an average recovery of 32 percent, which also dictated higher feed pressures around 73 psi at full capacity operation. The Well 3 tests operated at an average recovery of 25 percent with feed pressures of 67 psi at full capacity operation. Measuring the power supplied to the pump, there was little difference in average power (±5.8 percent) when the solar energy input exceeded 500 W, yet the NaCl test produced 25 percent more water than Well 3. The increased water production for NaCl is likely a result of primarily the differences in operating recovery. The NaCl solution has a slightly higher osmotic pressure to overcome and was operating at a higher operating recovery. Given the nearly vertical pump curve for the installed unit, there was little change in flow at the different operating feed pressures. To better evaluate the effect of water quality on the system operating curve, a modified experimental design is needed to eliminate confounding effects and test water qualities with greater differences in osmotic pressure.

5.3 System Component Case Study

This final case study evaluates how the characteristic operating curve for the system changes as a result of system component changes. In the first two case studies, the same system was used but the orientation, water quality, and operating recovery changed.

5.3.1 System Configuration and Testing Conditions

In this example, a different pump, pump controller, and membrane is used with the same feed water. The system components are summarized in table 18 and the PV panel orientation is specified in table 19.

Table 18.—System Information for 2014 Tests

Component	Brand/Model	Specifications
PV Panels	Grape Solar GS-S-100-TS	3 panels Total cell area: 1.5 m^2 Maximum power: 100 W per panel
Pump	Dankoff 1303-24	1/5 hp, 24 VDC Max flow: ~7.4 L/min Max total dynamic head (TDH): ~104 psi
Electrical Controller	Dankoff Pump Controller Model: DSP 200	Directly coupled to PV
Membrane	Membrane brand is unknown. Used membranes that came with the RO system.	Nominal Active Surface Area: 5 m^2 Material: thin film composite

Table 19.—Summary of Test Variables for System Component Case Study

Test No.	Day	Location	Water	Panel Azimuth	Panel Angle
4	6/17/2015	Alamogordo, NM	2 g/L NaCl	True South	36°
5	2/28/2014	Denver, CO	2 g/L NaCl	136°	53°

5.3.2 Feed Water and Operating Conditions

The feed water for the February 2014 testing was composed on 2 g/L NaCl added to municipal tap water. Compared to the water quality characteristics from section 5.2, the feed water conductivity was systematically about 6.5 percent higher during the 2014 testing (4046 ± 184 µS/cm) compared to the 2015 testing (3798±81 µS/cm). This difference in conductivity will lead to small differences in osmotic pressure between the two feed waters.

Both systems were operated with different recoveries during the test periods. For test 4, recovery was held constant around 32 percent (±0.16 percent). For test 5, recovery at the maximum permeate production was between 30 to 32 percent in good agreement with the operating recovery for test 4. As solar insolation on the panel decreased, recovery decreased, leading to a wider distribution in operating recovery between the two (2) tests (figure 27).

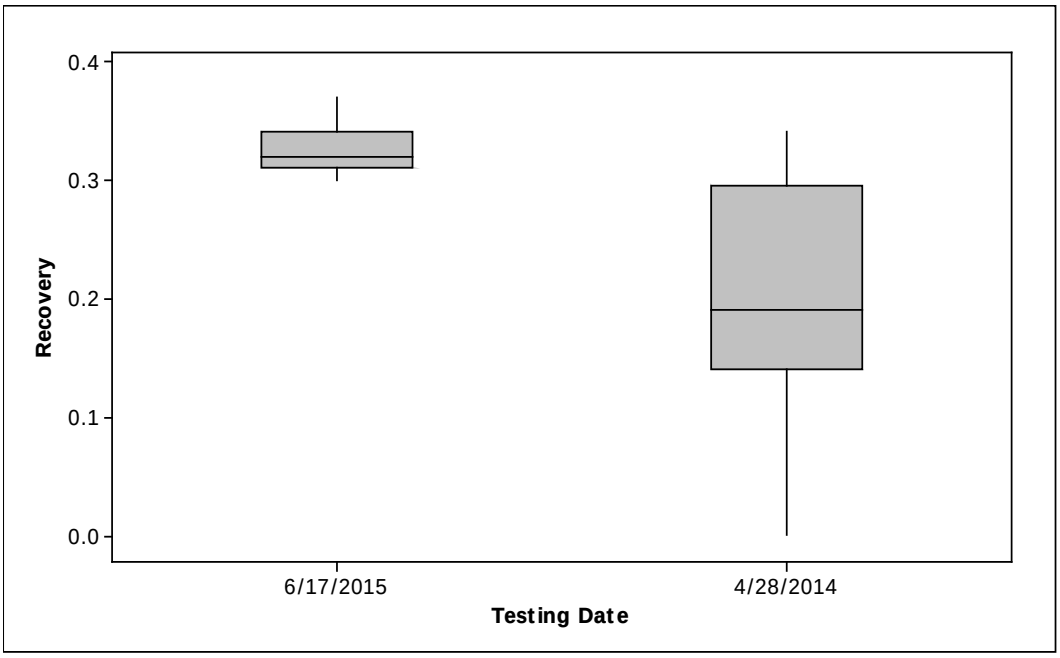

Figure 26.—Permeate recovery for NaCl test No. 4 and 5.

5.3.3 Evaluation of System Component Effects

The relationship between energy input and permeate production depends on system components. Figure 28 shows that the system utilized in test 4 produced more water per unit energy input compared to test 5. The maximum solar energy input of test 5 (788 W) was significantly less than test conducted in the same location (tests 2 and 3) due to differences in season (February *vs.* June).

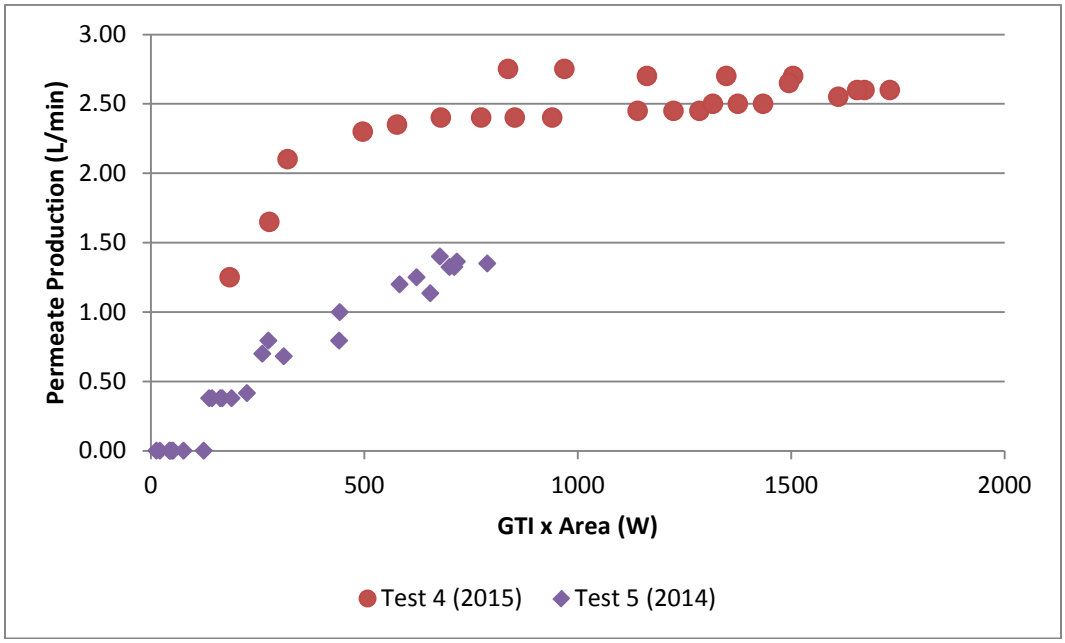

Figure 27.—Operating curves for tests 4 and 5 conducted with different system components and locations.

Several factors contribute to the differences in energy efficiency between systems. The membrane in test 5 was a standard reverse osmosis thin film composite membrane which required a higher operating pressure (108 psig) to achieve 30 percent recovery compared to the NF-90 membrane (72 psig). Differences in pump efficiency and pump controllers are apparent when analyzing the behavior at low solar energy inputs. For test 4, the pump was more efficient at low energy inputs and started to produce permeate at energy inputs less than 100 W. The pump used in test 5 did not produce any flow until the solar energy input exceeded 150 W. The pump controller in test 4 limited the power sent to the pump once the solar input exceeded 500 W, but no limitations were observed during test 5.

Since system components dictate the energy efficiency of a given system, this approach of developing a characteristic curve relating permeate production to solar energy input can illustrate system capability under different solar insolation conditions. Systematically modifying specific components and evaluating the change in the characteristic curve may yield insight into the incremental changes

under different environmental conditions. For example, changes in pump and pump controller components would change the ability of the system to utilize low-light conditions compared achieve maximum operating capacity under full sun conditions. Understanding energy utilization at different solar energy input levels is important for optimizing systems for different geographical locations and annual variations in solar energy input.

6. Conclusions and Recommendations

Solar energy is an increasingly important energy source for driving desalination processes. There is increasing interest in developing solar-driven desalination systems with a target niche of small community installations for brackish water desalination. With an increasing number of research studies published investigating solar desalination processes, there lacks a standard methodology for quantifying solar energy input. This study investigated different solar modelling approaches to develop a system operating characteristic curve relating solar energy input to water production.

Adequately quantifying solar energy to a solar desalination system requires careful consideration of system geometry and orientation. Simply measuring GHI with a pyranometer is not sufficient for reporting solar energy available for desalination processes. This study demonstrated that applying an isotropic solar model with direct and diffuse component estimates is necessary to adjust for differences in system location, orientation, and local time. With this model, permeate production as a function of solar energy input can be modeled within 20 percent.

For the PVRO system tested herein, the pump and controller components play an important role in energy utilization and experimental design. With a controller moderating the power sent to the pump, testing times immediately after dawn and before dusk were extremely important for evaluating performance during low-light conditions. Experimental design and testing procedures had to conform to capture these responses.

Predictably, the relationship between energy input and permeate production depends on the system components. Presenting data relating solar energy input to water production is an objective method for quantifying changes in system efficiency under different light conditions. For PVRO systems with fast system response times, the system operating curve presented herein may be more informative for visualizing the effect of different components than quantifying bulk ratios of electrical power generation to water production (kWh/m^3). The user can determine how components affect the utilization of low-light and maximum operating capacity in terms of water production. The operating curve

approach allows for the prediction of water production given GHI measurements and system orientation information.

This study presents a preliminary approach that requires additional testing to refine. A next important step is determining how to collect data during cloud events by adequately quantifying solar energy input during such events. It is inefficient to limit testing to full sun days from a time management and practicality standpoint. In many places, desalination systems are expected to produce water during cloudy conditions. Future testing should include testing a unit during variable weather conditions with a pyranometer mounted at the panel array to measure GTI directly. A horizontal mounted pyranometer with a shadow band should also be tested to determine direct and diffuse components without relying on empirical models.

Additional testing should also include an expanded experimental matrix testing different water qualities and recoveries systematically. Developing a multi-parameter model that predicts water production for three (3) independent variables (i.e., solar energy input, recovery, and feed osmotic pressure) would be an important tool for comparing systems and tailoring system design to different end users.

While PVRO was the only technology tested in this study, future work is needed applying this approach to other technologies. Modifications may be necessary to relation solar energy input to water production for processes based on solar thermal energy (e.g., solar distillation). These processes have long response times and system performance is dependent on the cumulative energy input and ability of the system to store thermal energy (heat capacity).

The overarching recommendation from this study is that the solar desalination field needs a standardized method for quantifying and reporting solar energy input to a system that is applicability across different solar desalination processes (e.g., PV, solar thermal, hybrid systems). Performance metrics that only quantify water production in terms of electrical power generation cannot be easily translated to processes that use solar thermal energy in some form.

For approaches that do use pyranometers to measure solar irradiance, the current data reporting methods are inadequate to compare results between studies. There are inconsistencies in how the pyranometer is mounted and often mounting details (i.e., horizontal *vs* tilted) are not reported. Even when details are reported, presenting data in terms of raw pyranometer readings does not yield directly comparable results. Solar irradiance data needs to account for system geometry and orientation to the sun. Neglecting to present solar irradiance information in a form that is representative of the actual solar energy input to the system places the burden on the reader to attempt to compare performance of a given unit under different solar conditions.

References

Abdallah, S., Abu-Hilal, M., Mohsen, M.S., 2005. Performance of a photovoltaic powered reverse osmosis system under local climatic conditions. Desalination 183, 95–104. doi:10.1016/j.desal.2005.03.030

Ahmad, G.., Schmid, J., 2002. Feasibility study of brackish water desalination in the Egyptian deserts and rural regions using PV systems. Energy Convers. Manag. doi:10.1016/S0196-8904(01)00189-3

American Water Works Association, 2010. Water Quality & Treatment: A Handbook on Drinking Water, Sixth Edit. ed, Water Resources and Environmental Engineering Series. McGraw-Hill Education, New York.

Averyt, K., Meldrum, J., Caldwell, P., Sun, G., McNulty, S., Huber-Lee, A., Madden, N., 2013. Sectoral contributions to surface water stress in the coterminous United States. Environ. Res. Lett. 8, 035046. doi:10.1088/1748-9326/8/3/035046

Bilton, A.M., Kelley, L.C., Dubowsky, S., 2011a. Photovoltaic reverse osmosis — Feasibility and a pathway to develop technology. Desalin. Water Treat. 31, 24–34. doi:10.5004/dwt.2011.2398

Bilton, A.M., Wiesman, R., Arif, A.F.M., Zubair, S.M., Dubowsky, S., 2011b. On the feasibility of community-scale photovoltaic-powered reverse osmosis desalination systems for remote locations. Renew. Energy. doi:10.1016/j.renene.2011.03.040

Bourouni, K., Ben M'Barek, T., Al Taee, A., 2011. Design and optimization of desalination reverse osmosis plants driven by renewable energies using genetic algorithms. Renew. Energy. doi:10.1016/j.renene.2010.08.039

Cheah, S.-F., 2004. Photovoltaic Reverse Osmosis Desalination System [WWW Document]. Desalin. Water Purif. Res. Progr. Rep. #104.

Clarke, D.P., Al-Abdeli, Y.M., Kothapalli, G., 2013. The effects of including intricacies in the modelling of a small-scale solar-PV reverse osmosis desalination system. Desalination 311, 127–136. doi:10.1016/j.desal.2012.11.006

Deutsche Gesellschaft für Sonnenenergie, 2008. Planning and Installing Photovoltaic Systems: A Guide for Installers, Architects and Engineers, Planning and Installing Series. Earthscan.

Elasaad, H., Bilton, A., Kelley, L., Duayhe, O., Dubowsky, S., 2015. Field evaluation of a community scale solar powered water purification technology: A case study of a remote Mexican community application. Desalination 375, 71–80. doi:10.1016/j.desal.2015.08.001

El-Shaarawi, M.A.I., Al Awjan, H., Al Ramadhan, D., Hussain, M., 2011. Effect of thermodynamic limitations on PV initial cost estimations for solar-powered RO desalination. Desalination. doi:10.1016/j.desal.2011.03.021

Erbs, D., Klein, S., Duffie, J., 1982. Estimation of the diffuse radiation fraction for hourly, daily and monthly-average global radiation. Sol. Energy 28, 293–302.

Filmtec Membranes System Design [WWW Document], n.d.

Fiorenza, G., Sharma, V.K., Braccio, G., 2003. Techno-economic evaluation of a solar powered water desalination plant. Energy Convers. Manag. doi:10.1016/S0196-8904(02)00247-9

Garg, M.C., Joshi, H., 2014. Optimization and economic analysis of small scale nanofiltration and reverse osmosis brackish water system powered by photovoltaics. Desalination 353, 57–74. doi:10.1016/j.desal.2014.09.005

Ghermandi, A., Messalem, R., 2009. Solar-driven desalination with reverse osmosis: the state of the art. Desalin. Water Treat. 7, 285–296. doi:10.5004/dwt.2009.723

Helal, A.M., Al-Malek, S.A., Al-Katheeri, E.S., 2008. Economic feasibility of alternative designs of a PV-RO desalination unit for remote areas in the United Arab Emirates. Desalination. doi:10.1016/j.desal.2007.01.064

Herold, D., Neskakis, A., 2001. A small PV-driven reverse osmosis desalination plant on the island of Gran Canaria. Desalination 137, 285–292. doi:10.1016/S0011-9164(01)00230-2

Kargar Sharif Abad, H., Ghiasi, M., Jahangiri Mamouri, S., Shafii, M.B., 2013. A novel integrated solar desalination system with a pulsating heat pipe. Desalination 311, 206–210. doi:10.1016/j.desal.2012.10.029

Kelley, L.C., Dubowsky, S., 2013. Thermal control to maximize photovoltaic powered reverse osmosis desalination systems productivity. Desalination 314, 10–19. doi:10.1016/j.desal.2012.11.036

Khayet, M., Essalhi, M., Armenta-Déu, C., Cojocaru, C., Hilal, N., 2010. Optimization of solar-powered reverse osmosis desalination pilot plant using

response surface methodology. Desalination 261, 284–292. doi:10.1016/j.desal.2010.04.010

Kreider, J.F., Kreith, F., 1981. Solar Energy Handbook. McGraw-Hill, New York.

Lichtwardt, M.A., Williams, D.M., 2000. Solar-powered direct current electrodialysis reversal system. US 09/005,826.

Mohamed, E.S., Papadakis, G., 2004. Design, simulation and economic analysis of a stand-alone reverse osmosis desalination unit powered by wind turbines and photovoltaics. Desalination. doi:10.1016/S0011-9164(04)00159-6

Mohamed, E.S., Papadakis, G., Mathioulakis, E., Belessiotis, V., 2008. A direct coupled photovoltaic seawater reverse osmosis desalination system toward battery based systems - a technical and economical experimental comparative study. Desalination 221, 17–22. doi:10.1016/j.desal.2007.01.065

Myers, D.R., 2013. Solar Radiation: Practical Modeling for Renewable Energy Applications. CRC Press, Boca Raton, FL. doi:10.1038/058619a0

Nafey, A.S., Mohamad, M. a., El-Helaby, S.O., Sharaf, M. a., 2007. Theoretical and experimental study of a small unit for solar desalination using flashing process. Energy Convers. Manag. 48, 528–538. doi:10.1016/j.enconman.2006.06.010

National Renewable Energy Laboratory, 2000. Solar Position and Intensity (SOLPOS) Calculator [WWW Document]. URL http://www.nrel.gov/midc/solpos/solpos.html (accessed 1.7.15).

Orgill, J., Hollands, K., 1977. Correlation equation for hourly diffuse radiation on a horizontal surface. Sol. Energy 19, 357–359.

Pisello, A., Pignatta, G., Castaldo, V., Cotana, F., 2014. Experimental Analysis of Natural Gravel Covering as Cool Roofing and Cool Pavement. Sustainability 6, 4706–4722. doi:10.3390/su6084706

Richards, L. a, Richards, B.S., 2011. Renewable energy powered membrane technology: Salt and inorganic contaminant removal by nanofiltration/reverse osmosis. J. Memb. Sci. 369, 188–195.

Santamouris, M., 2013. Energy and Climate in the Urban Built Environment, BEST (Buildings Energy and Solar Technology). Routledge.

Sathyamurthy, R., El-Agouz, S. a., Dharmaraj, V., 2015. Experimental analysis of a portable solar still with evaporation and condensation chambers. Desalination 367, 180–185. doi:10.1016/j.desal.2015.04.012

Sathyamurthy, R., Kennady, H.J., Nagarajan, P.K., Ahsan, A., 2014. Factors affecting the performance of triangular pyramid solar still. Desalination 344, 383–390. doi:10.1016/j.desal.2014.04.005

Skoplaki, E., Palyvos, J. a., 2009. On the temperature dependence of photovoltaic module electrical performance: A review of efficiency/power correlations. Sol. Energy 83, 614–624. doi:10.1016/j.solener.2008.10.008

Taghvaei, H., Taghvaei, H., Jafarpur, K., Karimi Estahbanati, M.R., Feilizadeh, M., Feilizadeh, M., Seddigh Ardekani, a., 2014. A thorough investigation of the effects of water depth on the performance of active solar stills. Desalination 347, 77–85. doi:10.1016/j.desal.2014.05.038

APPENDIX A

WELL 3 CASE STUDY
SUPPLEMENTAL DATA

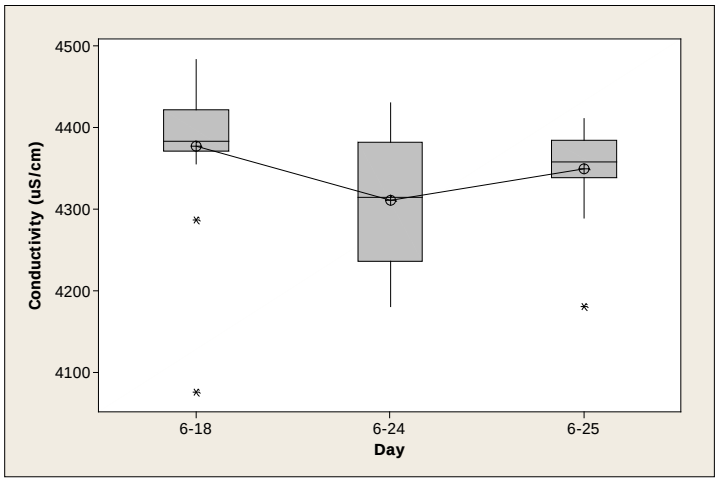

Figure A-1.—Box plot of feed water conductivities across each test day.
Box edges represent the 25% and 75% quartiles.

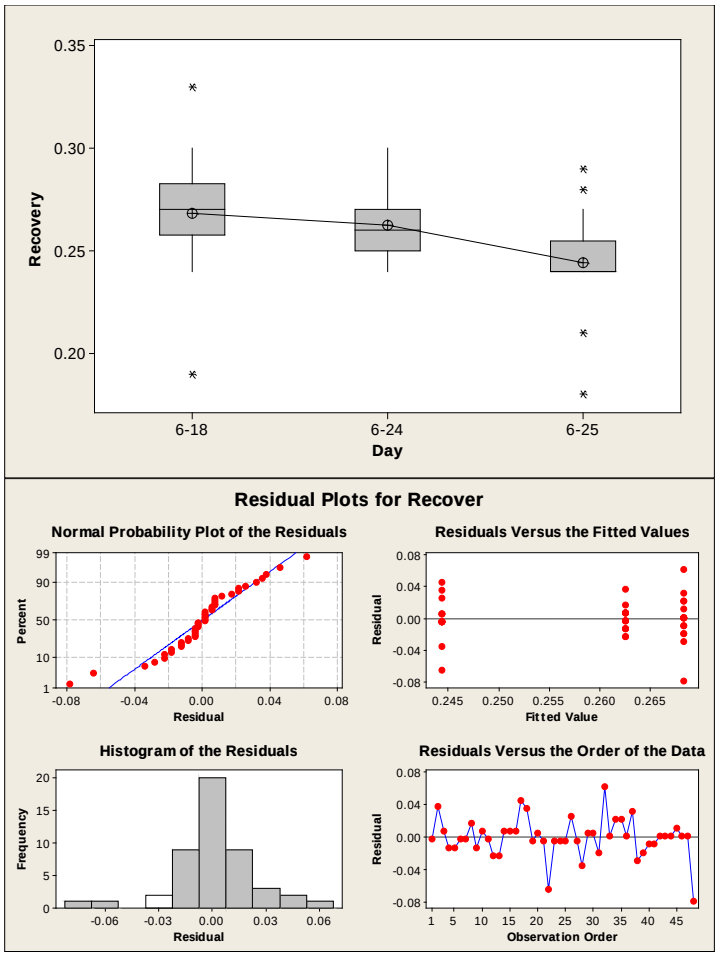

Figure A-2.—Box plot and residuals plot of permeate recovery across each test day.
Box edges represent the 25% and 75% quartiles.

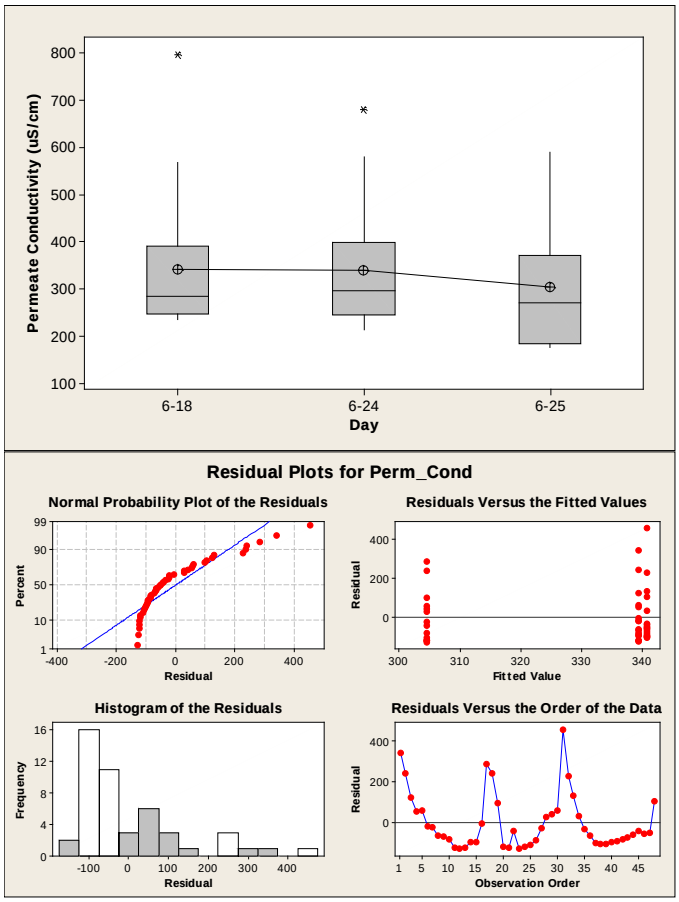

Figure A-3. Box plot and residuals plots of permeate conductivity across each test day. Box edges represent the 25% and 75% quartiles.

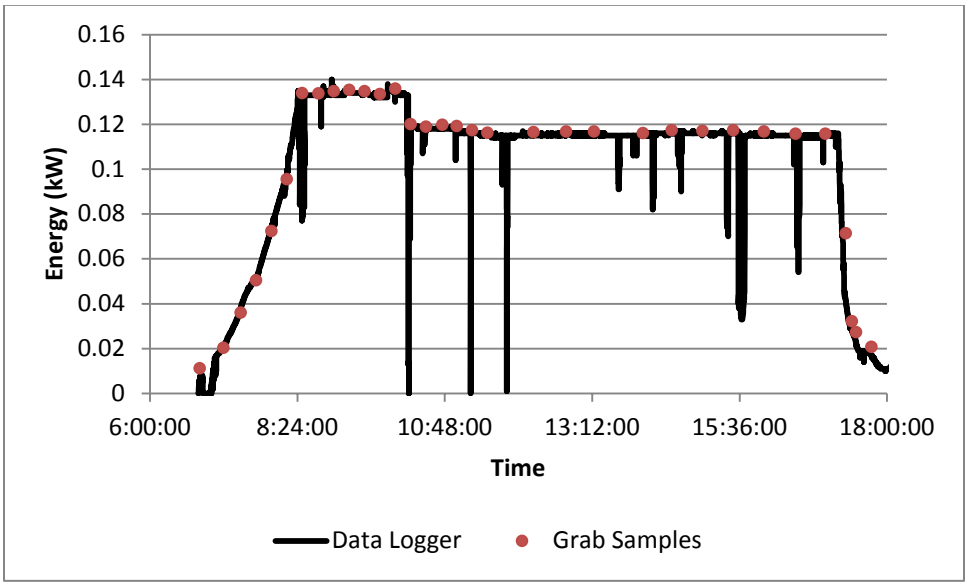

Figure A-4.—Power supplied to the pump as a function of time as measured by the data logger and manual measurements for testing on 6/17/15.

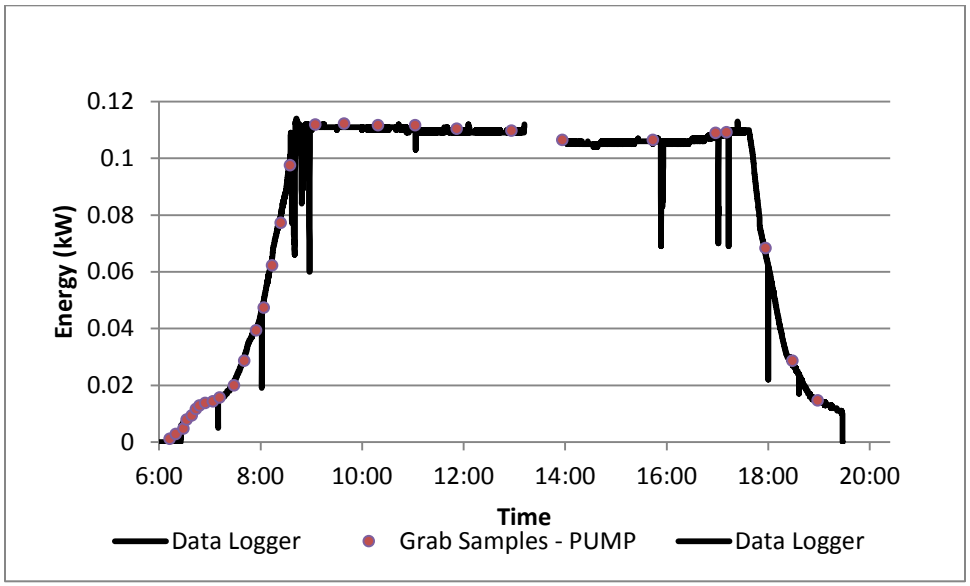

Figure A-5.—Power supplied to the pump as a function of time as measured by the data logger and manual measurements for testing on 6/18/15. Data logger data from 1:12 PM to 2:02 PM not shown due to logger malfunction. No data collected during this time.

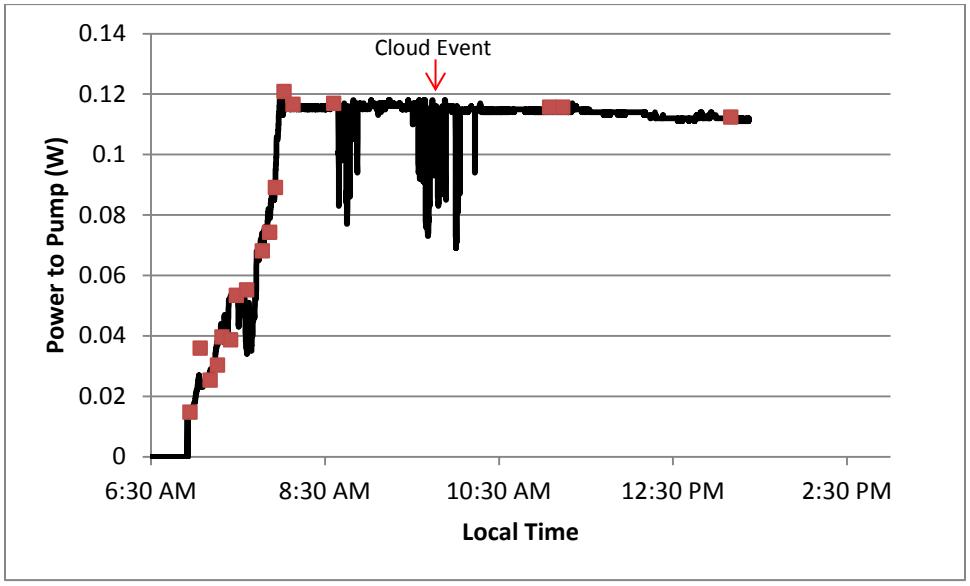

Figure A-6.—Power supplied to the pump as a function of time as measured by the data logger and manual measurements for testing on 6/24/15.

a)

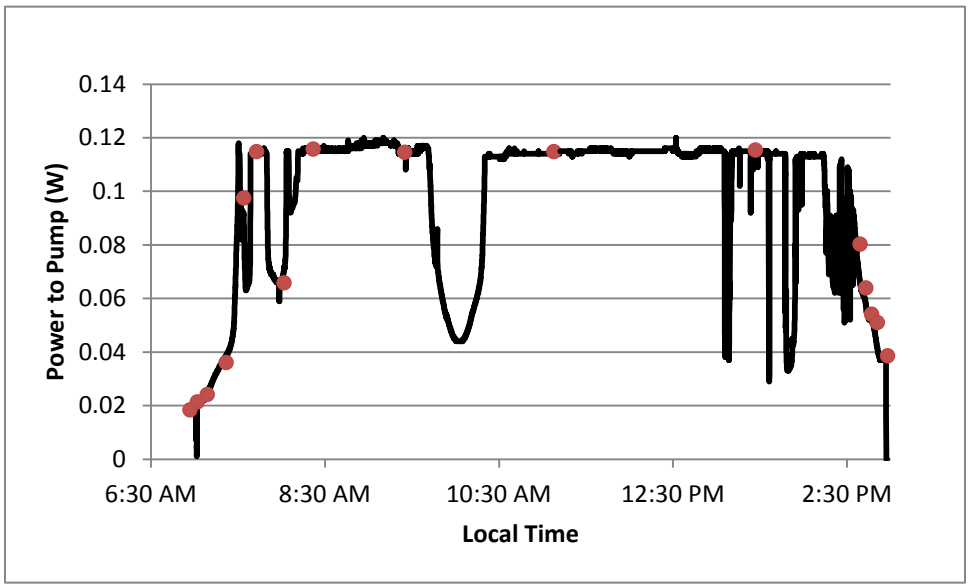

b)

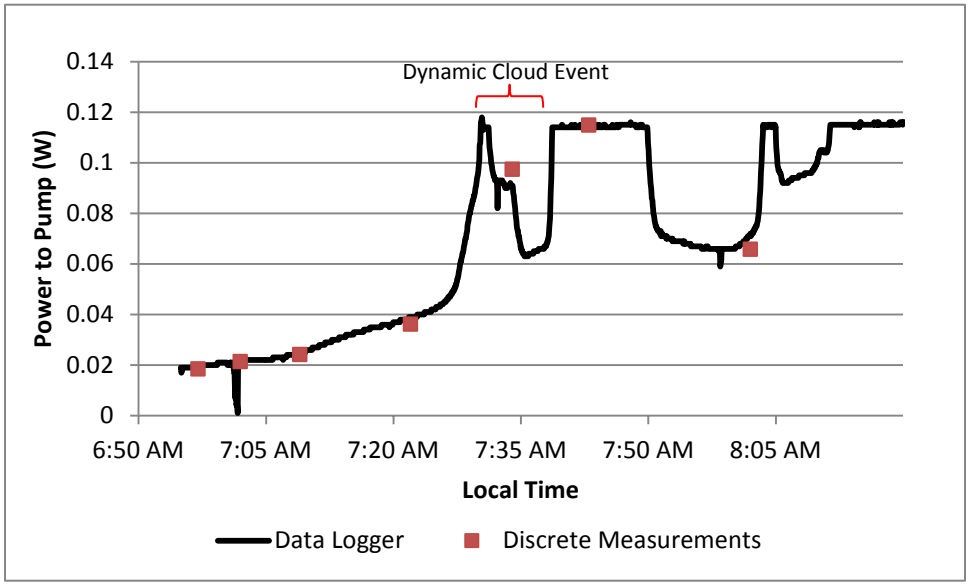

Figure A-7.—Power supplied to the pump as a function of time as measured by the data logger and manual measurements for testing on 6/25/15 for a) full testing day and b) early morning.

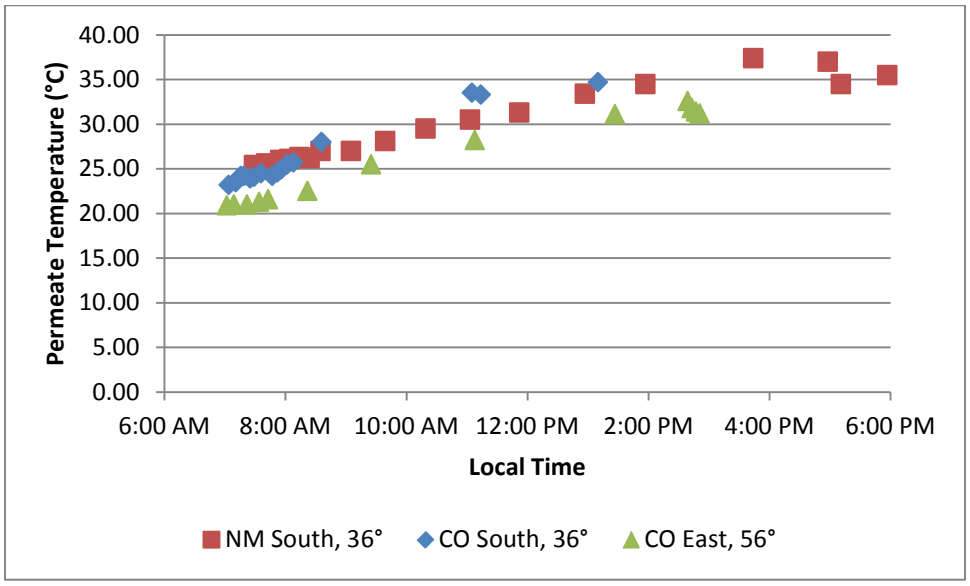

Figure A- 8.—Permeate temperature as a function of time for the 3 testing days

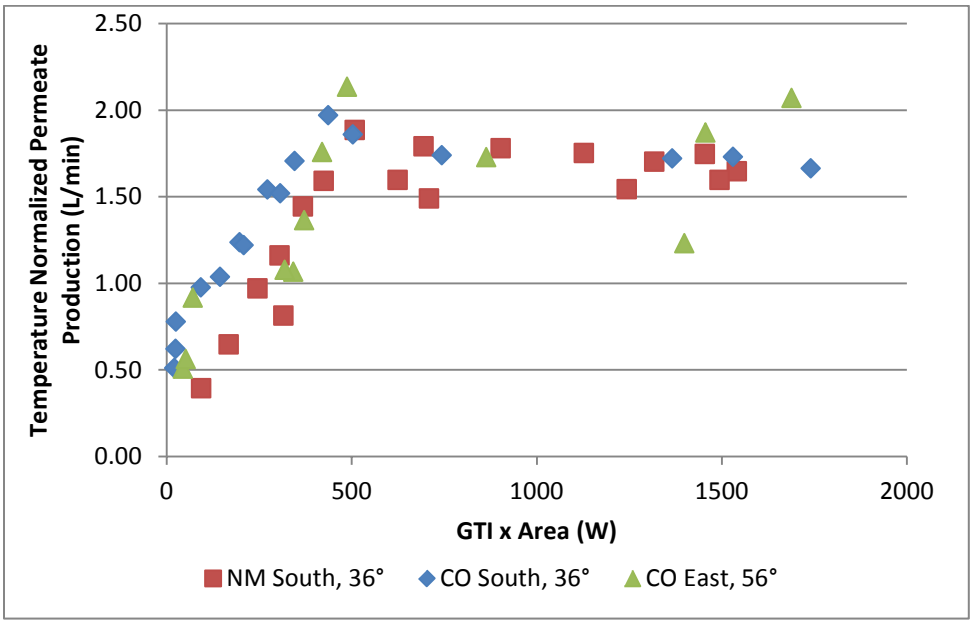

Figure A- 9.—Temperature normalized permeate production.